DROPLET MIGRATION ON CONICAL GLASS FIBERS

DROPLET MIGRATION ON CONICAL GLASS FIBERS

By

CLEMENTINE FOURNIER,
B.Sc. (ESPCI Paris)

A Thesis
Submitted to the School of Graduate Studies
in Partial Fulfillment of the Requirements
for the Degree
Master of Science

McMaster University

MASTER OF SCIENCE (2018)
(Physics)

McMaster University
Hamilton, Ontario

TITLE: Droplet migration on conical glass fibers

AUTHOR: Clementine Fournier,
B.Sc. (ESPCI Paris)()

SUPERVISOR: Dr. Kari Dalnoki-Veress

NUMBER OF PAGES: x, 51

Abstract

This thesis is centered on the study of spontaneous droplet migration along conical fibers. One of the key motivations for this project was to better understand the water-harvesting mechanism used by natural organisms like cacti. These desert plants exploit the conical shape of their spines to make fog condense into small droplets at the tip of theses spines. Then, droplets will spontaneously move towards the thickest end of the spines, bringing water to the main body of the plant. The key force behind drop migration on a conical fiber has been identified as the fluid surface tension by Lorenceau an Quéré in 2004 [1]. These authors also suggested and tested a model predicting the speed of drops on conical fibers. Here, we explore a larger range of relative sizes of drops compared to the fiber radius.

The present document describes how an experimental set-up was designed in order to study droplet migration with conical glass fibers and silicone oil droplets. Using optical microscopy and data analysis, the droplet speed was measured as well as the other experimental parameters. Finally, a simple theoretical model has been developed to predict the droplet speed as a function of geometrical parameters and fluid characteristics.

Preface

This thesis is divided in four chapters and falls into the category of "sandwich" thesis. This means that I incorporated the paper draft that resulted from my master project in the results section. The thesis starts with a introduction section in which all the necessary physical concepts are presented, namely the ones needed to understand the studied experimental system. The second section is devoted to the experimental methods that were used for this project as well as the data analysis performed. The third part, or results section, consists of the paper draft resulting from my master's work and a short introduction about this paper and my exact role in it. The last chapter presents a general conclusion about this work.

Acknowledgements

These two years as a MSc student at McMaster have been two amazing years and for that I have many people to thank. Kari, I want to start with you. Thank you for being a great supervisor as well as a great person. Discussing science with you was not only a learning opportunity, it was a pleasure. You taught me the most important lesson of all: the only way to achieve great things is by loving what we do. I will not forget that and I will not forget the example you set for me. Raffi, thank you for teaching me pretty much everything I know about droplets and fibers. Thank you for your patience, for helping me out (at least!) a thousand times and still being ready to come back again the next day. I don't think my master project would have turned out the same way if it wasn't for you being such a great mentor, always encouraging and positive.

I also want to thank everyone from the KDV lab for making these two years such an amazing experience. We shared drinks, crazy laughters and lab misfortunes and that itself has made it worthwhile. Carmen, I want to thank you in particular for indulging all my craziness and being the best mastermate ever.

A special thanks to everyone in the Physics department office. Rose, Cheryl, Hope, Tina, Mara, thank you for being there for me (and every student in the department!) and for making a huge difference on the small and big things alike. Mike and Dan, and every student in your group who lent a hand, thank you for taking the time to help and discuss with me.

Back in France, I want to thank my family and my friends for being so supportive, loving and amazing people. I crossed an ocean, but still thanks to you I never felt far from home. Yousra, thank you for being the best friend I never ever dreamt of having, my second brain, a better me. Lucas, I need to end this section with you. I don't think words are enough to explain how much I want to thank you, but I'll try. I can start with our endless discussions about research, you listening to so many talk practices, the fact that you've always been there for me, supporting me every step of the way. Thank you for being such a funny and interesting person, thank you for making life such a wonderful adventure. I am so grateful to have you.

Contents

List of Figures

Chapter 1

Introduction

The physics of small liquid objects such as drops or bubbles differs substantially from the physics used to describe larger fluid volumes or flows. For the latter inertia and gravity are crucial contributions that drive the fluid dynamics, in the case of drops and bubbles forces caused by surface tension and viscous dissipation come into play and can dominate inertial and gravity contributions [2]. These forces explain the original shapes and configurations that these small objects can have and therefore the many applications that result from these endless possibilities. In fact, academic work in the field of drops and bubbles is quite relevant for industries. Studies on the behavior of drops on flexible fibers networks [3–6], are of major interest to the textile industry. Works on the impact of drops on hydrophobic surfaces [7, 8] give a useful model for rain drops bouncing on a windshield or drops of pesticide sprayed on a leaf. Research on square droplets [9] can even be beneficial to other fields like optics, as they can be used as tunable lenses.

Surface tension and viscous dissipation are also responsible for some intriguing natural phenomena like the spontaneous motion of droplets on cactus spines [10] or on spider webs [11]. These phenomena were an inspiration for the work described in this thesis, which focuses on the spontaneous migration of droplets on conical fibers. Consequently, section 1.1 introduces surface tension, followed by a presentation of Laplace pressure, the overpressure that results from curved liquid surfaces. Then, the phenomenon of wetting and relevant fluid mechanics parameters for our systems are

described. Finally, the relevant theoretical models for a drop on a fiber (cylindrical and conical) are discussed.

1.1 Surface tension

1.1.1 Microscopic explanation

Before even defining what surface tension is, one needs to define what a liquid is. A liquid is commonly described as one of the three possible phases for a material: solid, liquid or gas. Liquid is the "in between" phase: it is condensed like a solid, but disordered like a gas. The necessary condition for its formation and stability is that molecular attraction overcomes thermal agitation. Now, if we look at individual molecules inside the liquid, we can divide them into two categories: the majority of them are in the bulk, having as many cohesive interactions with their neighbors as possible, the rest are at the interface and have only half of their interactions with their neighbors. Thus, a particle in the bulk is in a more energetically favorable configuration than a particle at the interface [2,12,13]. These two types of situations are depicted in Fig. 1.1.

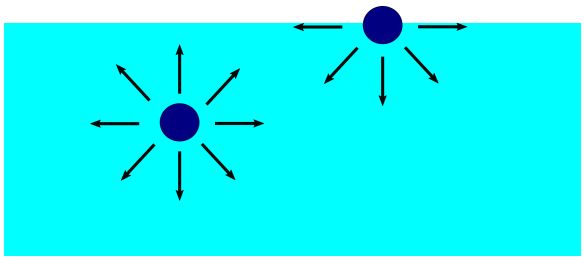

Figure 1.1: Schematic of two liquid particles illustrating the microscopic view of surface tension. The particle on the left is in the bulk of the fluid and has all its attractive interactions. Therefore, it is in a favorable configuration. On the contrary, the particle on the right is at the interface between liquid and gas and has only half of its interactions, thus is in a less favorable configuration.

The simple description of molecules at an interface and in the bulk explains intuitively why a liquid always has the configuration that minimizes its surface area while satisfying the other external conditions. If we call U the energy of one molecule in

the bulk, then a molecule at the interface has an energy of $U/2$. If the molecule has a characteristic size of a and thus a characteristic surface of a^2, then it is possible to define the surface tension γ as [2]:

$$\gamma = \frac{U}{2a^2}. \tag{1.1}$$

Here, the surface tension can be understood as the energy deficit of a molecule at the interface, per unit of surface area. Additionally, the energy deficit itself is often referred to as the surface energy. Thus, the surface tension is related to how a liquid at a curved interface will try to minimize its surface area [2,14]: the more γ increases, the less favorable it will be for a molecule to be at the interface and the more the surface area will decrease.

1.1.2 Macroscopic explanation: work and force

The surface tension can also be described macroscopically in terms of work and force. As we have seen in the previous section, it is unfavorable to have particles at the interface, so one needs to bring energy to the liquid to increase its surface area. γ is the direct measurement of how much energy per unit area one has to supply to increase the surface area by one unit. Accordingly, the work dW necessary to increase the surface by an amount dA can be written as:

$$dW = \gamma dA. \tag{1.2}$$

Similarly, γ can also be defined as a force per unit length which is applied to a liquid in order to minimize its surface area. A famous example that shows the role of γ as a force is the following one [2,12,15]: a mobile rod of length L acts as the fourth side on a three-sided frame, which is dipped into a soap-water mixture. The resulting frame whose surface is covered with a soap film is shown in Fig. 1.2.

As soon as the rod is let free, it starts to move towards the parallel side of the frame, in order to decrease the surface area of the film. In this situation, the surface tension can be presented as a force (per unit length) pulling the rod towards the liquid in the plane of the surface. In this case, one can write the following expression for the work

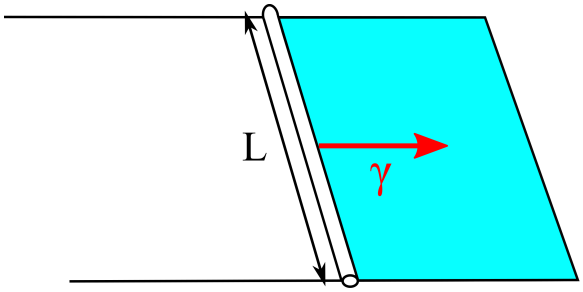

Figure 1.2: Schematic of a frame whose fourth side is replaced by a rod. Inside the frame is a thin film of soap that covers the whole surface. Once the rod is released, the rod will start to move towards the rest of frame in order to minimize the surface area and thus the surface tension.

dW applied on the rod:

$$dW = Fdx = 2\gamma L dx, \tag{1.3}$$

where F is the force applied on the rod, dx is the displacement of the rod. The factor of 2 is due to the two surfaces, top and bottom. Expression 1.3 illustrates not only that γ is the energy needed to increase the surface area by an amount of Ldx but also that the term $2\gamma L$ is a force.

1.1.3 Surface tension for a few common liquids

The most commonly used unit for surface tension is mN/m (because surface tension is a force per unit length) which is equivalent to mJ/m^2. Tab. 1.1 presents the surface tensions measured for 2 well-known liquids, water and mercury and two liquids used in the experiments presented in this thesis, glycerol and silicone oil [2,13].

Liquid	Water	Mercury	Glycerol	Silicone oil
γ (mN/m)	72	485	63	22

Table 1.1: Examples of surface tension for a few relevant liquids [2,13]

.

It is interesting to compare the values of the different surface tensions. For silicone

oil, the energy of one molecule is of the order of kT, which yields $\gamma \sim 20$ mN/m for a temperature close to 20°C. On the other hand, the energy of a water or glycerol molecule depends highly on the hydrogen bonds between molecules. The energy associated to hydrogen bonds is greater than the energy associated to Van der Waals forces, therefore water and glycerol have a higher surface tension than silicone oils. Finally, the mercury surface tension value is given to show the order of magnitude of one the highest γ that can be reached. Mercury surface tension is one order of magnitude bigger than the other surface tensions because metallic bonds are stronger than hydrogen bonds, which is also why mercury is one of the most cohesive liquids.

1.2 The Laplace pressure

1.2.1 Definition - Laplace theorem

One of the consequences of surface tension is the Laplace pressure. The Laplace pressure is the overpressure that exists inside drop and bubbles compared to the outside pressure. More generally, the Laplace pressure is the excess pressure found at a curved interface between two phases [2, 14]. An easy way to understand how Laplace pressure works is to look at a portion of a drop shown in 2D in Fig. 1.3.

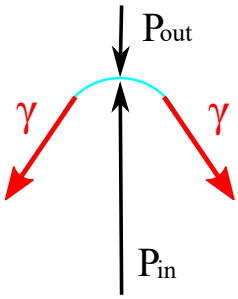

Figure 1.3: Schematic of the top part of a drop, showing the surface tension γ applying a force on both sides of the drop, thus creating a pressure P_{in} inside the droplet higher than the outside pressure P_{out}.

On both extremities of the interface of this drop portion, there is a force applied by the rest of the drop due to surface tension. As seen in section 1.1, γ can be described as a force per unit length minimizing the surface area of the liquid, which explains

that it "pulls" on both sides of this drop portion to flatten its surface. As a result, the pressure inside the drop P_{in} is higher than outside P_{out}. The Laplace pressure ΔP can then be defined as:

$$\Delta P = P_{in} - P_{out}. \tag{1.4}$$

A general expression of ΔP as a function of γ for all types of curved surfaces is given by the Laplace theorem [2, 16]:

$$\Delta P = \gamma \left(\frac{1}{R} + \frac{1}{R'} \right), \tag{1.5}$$

where R and R' are the radii of curvature of the interface in 3D.

In the case where the interface is a sphere, e.g. a drop of water in oil, the expression of ΔP as a function of γ can be derived simply [2, 16]. One can start by dividing mentally the drop into two hemispheres with the same radius r. The forces applied on a given hemisphere are F_γ, the force applied by surface tension on the contour shared with the other hemisphere (see Fig. 1.3) and F_P, a force applied by the pressure in the other hemisphere on the whole surface area shared by the two halves of the drop. Because the system is at equilibrium, these two forces are equal. Thus we have:

$$F_\gamma = F_P, \tag{1.6}$$

which can then be rewritten as:

$$2\pi r\gamma = \Delta P \pi r^2, \tag{1.7}$$

because the pressure applied to the hemisphere is exactly the difference $P_{in} - P_{out}$ that was defined as ΔP in Eq. 1.4. Eq. 1.7 can itself be rewritten to give the expression of ΔP for a sphere:

$$\Delta P = \frac{2\gamma}{r}. \tag{1.8}$$

Therefore, the smaller the drop, the larger ΔP and thus the less thermodynamically stable the drop is. It is interesting to see that the Laplace pressure gives a direct measure of how stable a curved interface is. Spontaneously, a system always undergoes changes that minimize ΔP when possible. Thus the Laplace pressure can be a convenient parameter to use to explain changes in a bubble shape or the spontaneous migration of drops. The Laplace pressure is used in a later section (see section 1.6.1) to account for the spontaneous motion of drops on conical fibers.

1.2.2 Minimal surfaces

A consequence of the existence of surface tension (and Laplace pressure) is that a liquid at a curved interface always changes shape and configuration in order to minimize its surface area and also in order to decrease the Laplace pressure. One of the shapes that most often satisfies these conditions is a spherical shape. The spherical shape explains common physical phenomena that can be observed in everyday life. For instance, the stream of water coming out of a faucet usually breaks into several droplets, because the surface area of the equivalent cylinder of fluid is larger than the cumulated surface area of these drops (Plateau-Rayleigh instability) [2]. Another good example of the minimal surfaces reached by a fluid is the one of a drop sitting on a fiber. If some conditions are met, the fluid envelopes the fiber and takes the shape of a barrel, to minimize its surface area in contact with air. We discussed minimal surfaces in more details in section 1.5.1 and depict them in Fig. 1.5.

1.3 Wetting and contact angle of a drop

When a liquid drop is deposited on a solid surface (or on top of an immiscible liquid), three different interfaces are created: solid-liquid, liquid-gas and solid-gas. Depending on the characteristics of these three interfaces, the drop takes a defined shape: the study of the shape is called wetting. For instance, a water drop spreads on glass,

while a mercury drop remains quasi spherical. On the contrary, a water drop on a polyethylene sheet doesn't spread [13]. From these examples, we see that there are two main types of wetting: total wetting, where the drop spreads completely on the solid because of its strong affinity with it, and partial wetting, where the drop forms a spherical cap on top of the solid. These two types of wetting are depicted in Fig. 1.4.

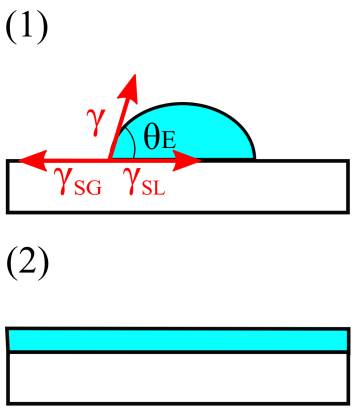

Figure 1.4: Schematic of the two types of liquid wetting on a solid substrate: (1) partial wetting and (2) total wetting. In the case of (1), one can define the contact angle θ_E between the droplet surface and its contact line with the solid substrate. Also shown in (1) are the different surface tensions in the system: γ is the tension at the gas/liquid interface, γ_{SG} the one at the gas/solid interface and γ_{SL} the one at the solid/liquid interface.

To know if a liquid drop spreads on a given solid, one needs to know the value of the spreading parameter, or wetting coefficient, S [2,12,15]. S characterizes the difference of surface energy (defined in section 1.1.1) per unit area between the dry substrate and the wet substrate, in other words the difference of surface tension. When the substrate is dry, the only existing surface tension is the surface tension at the solid/gas interface, γ_{SG}. On the contrary, when the substrate is wet, there are two different surface tensions: a surface tension at the liquid/gas interface, γ, and a surface tension at the solid/liquid interface, γ_{SL}. Therefore, S is:

$$S = \gamma_{SG} - (\gamma + \gamma_{SL}). \tag{1.9}$$

Again, the system evolves in the direction that minimizes its total surface energy. In

the case where $\gamma_{SG} > (\gamma + \gamma_{SL})$, which is equivalent to say that a dry substrate is less energetically favorable than a wet substrate, the liquid spreads completely. The wetting is total and is defined by $S > 0$. On the other hand, when $S < 0$, then a wet substrate is less energetically favorable than a dry one. The drop takes the shape of a spherical cap and the wetting is partial. Therefore, the angle between the solid/liquid interface and the liquid/gas interface is defined as the contact angle of the drop and noted θ_E [2, 13]. The contact angle is shown in Fig. 1.4. When the wetting is total, θ_E is equal to 0, as there is no spherical cap but only a thin liquid film.

It is possible to derive θ_E when the wetting is partial and the three different interfacial tensions are known, using the law of Young-Dupré [2, 15]. One can sum all the capillary forces applied on the point where the three interfaces meet (also know as the triple line). These capillary forces are depicted in Fig 1.4. At equilibrium, the sum of these forces is equal to zero. The projection of these capillary forces normalized by unit length onto the horizontal direction, i.e. the substrate plane, yields the following equation:

$$\gamma \cos(\theta_E) = \gamma_{SG} - \gamma_{SL}. \tag{1.10}$$

Eq. 1.10 enables the experimentator to find the contact angle of the drop on a plane surface if all surface tensions are known. Eq. 1.10 can alternatively be written as a function of S.

1.4 Relevant fluid mechanics parameters

When working with fluids at a small scale, one of the challenges is to be able to evaluate which forces are relevant and which aren't. Therefore, it is necessary to identify and use dimensionless parameters whose value gives a comparison of two forces. In our case, two parameters are particularly significant: the capillary length and the Reynolds number.

1.4.1 Influence of gravity: the capillary length

The capillary length, or capillary constant, is used to compare capillary forces to gravity [2, 15]. The capillary length is a characteristic length noted κ^{-1} under which gravity doesn't have an impact on the studied fluid object while capillary forces are significant. On the other hand, when the studied object has higher dimensions than κ^{-1}, then gravity matters and influences the object shape.

To derive an expression for κ^{-1}, one has to consider that when the object (e.g. a drop) has a characteristic length of κ^{-1}, then both capillary forces and gravity are important. Therefore, at equilibrium, the pressure created by the surface tension γ/κ^{-1} (Laplace pressure) is equal to the hydrostatic pressure $\rho g \kappa^{-1}$, where ρ is the fluid density and g the standard acceleration due to gravity [12]. By balancing these contributions, we have the following expression for κ^{-1}:

$$\kappa^{-1} = \sqrt{\gamma/\rho g}. \tag{1.11}$$

Capillary lengths calculated for a few relevant liquids are shown in Tab. 1.2.

Liquid	Water	Mercury	Glycerol	silicone oil
κ^{-1} (mm)	2.7	1.9	2.3	1.5

Table 1.2: Examples of capillary lengths for a few relevant liquids [17]

.

These capillary lengths are all on the order of a few millimeters, which means that drops of these liquids need to have a diameter smaller than a millimeter to be in a regime where gravity can be neglected when compared to surface tension.

1.4.2 Fluids dynamics approach: the Reynolds number

Because we consider moving drops in our study, we need to have a fluid dynamics approach to the problem. Just like Newton's second law for solid objects, there is a set of equations that can be applied to all types of fluids to describe their dynamics (i.e.

their flow): the Navier-Stokes equations. Section 1.4.2 briefly introduces the Navier-Stokes equations and then describes how they can be used to define the Reynolds number, which is employed to compare the relative magnitude of the inertia of a fluid versus the viscous drag applied to that same fluid.

The Navier-Stokes equations

The Navier-Stokes equations can be written as [18]:

$$\rho\left(\frac{\mathrm{D}\mathbf{v}}{\mathrm{D}t}\right) = \rho\left(\frac{\mathrm{d}\mathbf{v}}{\mathrm{d}t} + \mathbf{v}\cdot\nabla\mathbf{v}\right) = -\nabla p + \eta\nabla^2\mathbf{v} + \mathbf{f}, \tag{1.12}$$

where $\mathbf{v}$ is the velocity field of the studied unit of fluid. In 3 dimensions, with a cartesian coordinates system (x, y, z), $\mathbf{v} = (v_x, v_y, v_z)$. Moreover, p is the pressure applied to that unit, η is the viscosity of the fluid and $\mathbf{f}$ is the sum of the other external forces, or body forces, applied to that unit (e.g. gravity). Eq 1.12 is equivalent to a set of 4 equations: one for each component of $\mathbf{v}$ and the continuity equation which states that the fluid mass is conserved. In the case where the fluid is incompressible, Eq 1.12 can be simplified (because $\nabla\mathbf{v} = 0$):

$$\rho\left(\frac{\mathrm{d}\mathbf{v}}{\mathrm{d}t}\right) = -\nabla p + \eta\nabla^2\mathbf{v} + \mathbf{f}. \tag{1.13}$$

The Navier-Stokes equations are complex. These equations are partial differential equations that are of the second order and non-linear. To solve them, extra information is needed, such as boundary conditions. For instance a common boundary condition is the no-slip boundary condition, which means that if a fluid is in contact with a solid surface, the fluid at the contact line has the same velocity as the solid.

However, as stated in the introduction of section 1.4.2, one can intuitively understand the Navier-Stokes equations as an equivalent of Newton's second law applied to a fluid unit [18]. On the left hand side of Eq. 1.12, there are the inertial terms. The inertial terms are comparable to the ma term in Newton's law: ρ accounts for the mass of the fluid normalized by a volume unit, while $\frac{\mathrm{D}\mathbf{v}}{\mathrm{D}t}$ contains the two terms corresponding to the acceleration, both the time derivative of the velocity field and the convective

acceleration term. On the right hand side, the terms are all forces (normalized by a volume unit) applied to the fluid unit: the pressure gradient $-\nabla p$, the viscous drag $\eta\nabla^2\mathbf{v}$ and other forces like gravity $\mathbf{f}$.

The Reynolds number

Knowing the Navier-Stokes equations, we can express a dimensionless parameter that will define different flow regimes in fluid mechanics. This dimensionless parameter is known as the Reynolds number Re and is a ratio of the inertial term of Navier-Stokes equations (inertial forces) to the viscous forces [18]. In the case where $\mathrm{Re} \ll 1$, the viscous forces overcome the inertial forces and the fluid has a smooth, regular motion. The flow is defined as laminar. On the other hand, when $\mathrm{Re} \gg 1$, then the viscous forces are negligible compared to the inertial forces. In the case where $\mathrm{Re} \gg 1$, the flow is characterized as chaotic and can produce instabilities such as vortices. Such a flow is defined as a turbulent flow. An expression for Re is given by:

$$\mathrm{Re} = \frac{\rho L V}{\eta}, \tag{1.14}$$

where V is a typical flow speed and L a characteristic lengthscale of the flow.

We can fully derive Re by making the whole Navier-Stokes equation non-dimensional and then observe how Re spontaneously appears as the coefficient in front of the viscous forces term. But we can also understand where Eq. 1.14 comes from just by looking at the ratio $|inertia\ term|/|viscous\ term|$. Let's keep the variables V and L defined in Eq. 1.14. We assume that any spatial derivative of $\mathbf{v}$ is of the order of V/L, which means that the velocity $\mathbf{v}$ varies of an amount V over lengthscales on the order of L. Similarly, a second order spatial derivative of $\mathbf{v}$ is of the order of V/L^2. We can now rewrite the two terms of the ratio [18]:

$$|inertia\ term| = |\rho\mathbf{v}\cdot\nabla\mathbf{v}| = O(\rho V^2/L), \tag{1.15}$$

$$|viscous\ term| = |\eta\nabla^2\mathbf{v}| = O(\eta V/L^2). \tag{1.16}$$

Consequently, we can express the ratio itself using Eq. 1.16:

$$\frac{|inertia\ term|}{|viscous\ term|} = O\left(\frac{\rho V^2/L}{\eta V/L^2}\right) = O\left(\frac{\rho LV}{\eta}\right) = O(\mathrm{Re}). \tag{1.17}$$

Thus, we can understand how Re is the parameter to evaluate which one of the inertial term or the viscous term overcomes the other. In our study, the evaluation of Re enables us to neglect the inertial forces and simplify our model. That is, in the study presented here, flow velocities are small enough that we have laminar flow.

1.5 Drop on a cylindrical fiber

The four previous sections presented a series of general concepts necessary for the understanding of our system, which is a liquid drop on a solid conical fiber. In section 1.5, we introduce a simpler but important system that will help us describe our own system: a drop on a cylindrical fiber. First, the two possible configurations a drop can take on a cylindrical fiber, clam-shell and barrel, are highlighted. Then we present the framework with which a drop on a cylindrical fiber can be described and the derivation of the drop profile. We want to acknowledge here that a decisive contribution was made by B. Carroll [19,20], who built the comprehensive framework for a drop on a cylindrical fiber and was the first to derive the drop profile.

1.5.1 Barrel and clam-shell: two possible drop shapes

Let's consider a case where gravity is negligible. When a liquid drop is brought in contact with a cylindrical fiber, there are two extreme possible shapes that the drop can take: a barrel shape, where the liquid envelopes the fiber, or a clam-shell shape where the drop is only on one side of the fiber. The essential difference is that a barrel-shaped drop is axisymmetric, while a clam-shell drop isn't. Both configurations are depicted in Fig. 1.5. A drop can also undergo a transition from a barrel shape to a clam-shell shape and take intermediate shapes if the right conditions are met and we describe these conditions next [20,21].

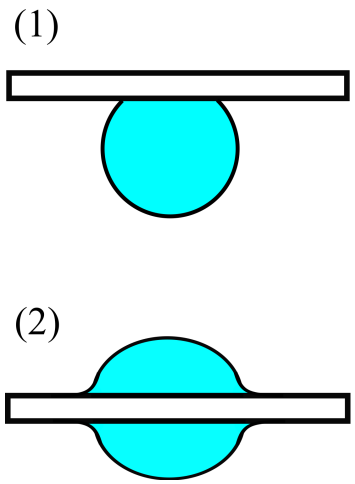

Figure 1.5: Schematic of the two types of shape that a drop on a fiber can take (side view): (1) clam-shell and (2) barrel. For (1), the droplet is only on one side of the fiber whereas for (2) the droplet is axysymetric and envelops the fiber entirely.

There are two important factors impacting which configuration will be favored: the reduced volume of the drop (the drop volume divided by the fiber radius cubed) and the equilibrium contact angle between the liquid and the solid [20–22]. The influence of both the reduced volume and the contact angle can be understood intuitively. For the reduced volume of the drop, the larger it is, the easier it will be for the drop to fully envelop the fiber. The influence of the reduced volume has been shown by both Carroll and McHale [20, 23]. These authors performed similar experiments where the reduced volume of the drop decreases while the contact angle is kept the same. The reduced volume volume diminution was done either by decreasing the volume of an oil drop in a water bath with the addition of surfactants [20], or by increasing the fiber radius [23]. In both cases, the drop undergoes a transition from a barrel to a clam-shell shape, which is a roll-up transition.

On the other hand, the smaller the contact angle is, the more affinities the liquid has with the solid, therefore the more chances the drop has to have a barrel shape, as the barrel shape maximizes the solid-liquid contact. Theories were developed that link the barrel to clam transition point to a critical contact angle [20–22], even though these models don't quite match the literature data available. In fact, the experimen-

tal reduced height of the drop at the transition is systematically above the expected transition height. Some authors instead proposed another critical condition signalling the transition from barrel to clam-shell: when the inflexion point of the drop profile touches the fiber surface [21]. But here again, there is still a discrepancy with the experimental data.

As of today, there is no single model that describes fully the transition nor predicts which configuration a given drop will take on a fiber [21, 24]. Some authors have observed that both barrel and clam-shell drops can coexist in some cases, even in the equilibrium state [24]. The transition from barrel to clam is a difficult theoretical problem, because even if the profile of a barrel drop can be thoroughly predicted using a differential equation [19], there is no such model for the clam-shell drops. New methods such as finite-element simulations have been used more recently [24] to approach the problem. In the present study, we will limit ourselves to the simpler case of a barrel drop and the model for a barrel drop profile is presented in the next section.

As a side note, when gravity matters, the liquid conformation can change, as the drop will lean downwards. In fact, gravity modifies the phase diagrams of a drop on a fiber [24]. However, the case where gravity matters is not relevant to our study, as we consider the case where gravity is negligible (when the length scale of the droplet is inferior to the capillary length, see section 1.4.1).

1.5.2 Theoretical framework and profile of a barrel drop

When we consider a barrel drop on a fiber, there are several parameters that need to be defined [19]: the radius of the fiber r, the maximum height of the drop h, the overpressure inside the drop or Laplace pressure ΔP. These variables are shown in Fig. 1.6.

Another important parameter of the drop on cylindrical fiber system is the contact angle between the drop and the fiber. Here, there is an essential difference between a flat and a cylindrical surface. Even with a zero contact angle, there can still be a drop profile on a cylindrical fiber. The air/liquid profile line connects smoothly with

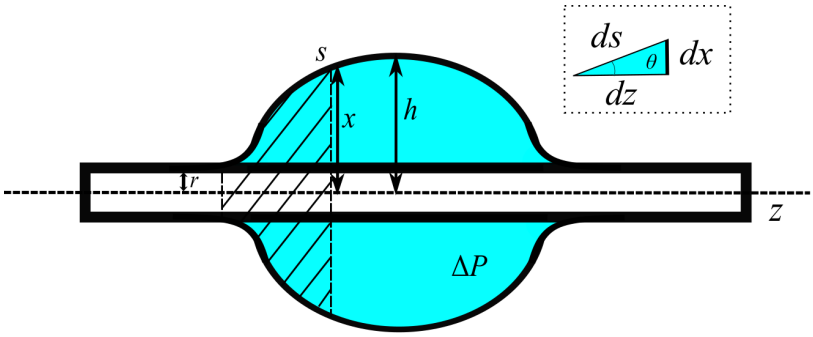

Figure 1.6: Schematic of a barrel-shaped drop on a cylindrical fiber (side view). Here are displayed the radius r of the fiber, the maximum height of the droplet h, its height at a random point on the surface x and its corresponding curvilinear coordinate s, and the Laplace pressure of the drop ΔP. The hatched area between the extremity of the drop and the line originating from that random point on the surface denotes the volume on which force derivations are made to determine the drop profile. The inset depicts the angle θ between a small displacement ds and the z-axis.

the solid at the triple line, as depicted in Fig. 1.6. On a microscopic level, there is a thin film of liquid enveloping the fiber on both sides of the drop. In section 1.5.2 and in the rest of the present study, we consider a zero contact angle, which is the contact angle obtained for a silicone oil drop on a glass fiber.

There are two ways to derive the profile of a drop on a cylindrical fiber. The first derivation method is based on solving the equation given by the Laplace theorem (see section 1.2.1) applied to the drop [2, 12, 19]. The second derivation method uses a force approach and is the method presented here, as given by de Gennes, Brochart and Quéré [2]. Let's consider a portion of the drop, starting from the extremity to an intermediate position before the middle of the drop. The height of the drop at the intermediate position is x, while the drop coordinate on the horizontal axis (or z-axis) is z. The drop curvilinear coordinate (following the contour of the drop) is s. x, z, s and the portion of the drop of interest, which is displayed as a hatched area, are shown in Fig. 1.6. We also need to introduce the angle θ, shown in the inset of Fig. 1.6. θ is the angle between a curvilinear displacement ds and the horizontal direction or z-axis. A displacement ds corresponds to a vertical displacement dx and a horizontal displacement dz.

Because the drop is at equilibrium, we know that the sum of the forces applied on the hatched portion of the drop and projected onto the z-axis is zero. There are three different forces applied on the drop. The first force, that we call f_1, is the capillary force caused by the surface tension in the rest of the drop on the portion of interest. f_1 is applied on the right side of this portion, on the external contour line that is in contact both with the rest of the drop and the air. f_1 is proportional to γ, as well as the perimeter of this contour line, namely $2\pi x$ and because we project f_1 onto the z-axis, f_1 is also proportional to $\cos(\theta)$:

$$f_1 = 2\pi x \gamma \cos(\theta). \tag{1.18}$$

On the same side of the portion of the drop as f_1, but on the opposite direction, there is also a second force, f_2. f_2 is created by the pressure ΔP inside the rest of drop and is applied on the right side surface of the portion of interest. This surface is the surface of the drop itself πx^2 to which we need to subtract the surface of the fiber πr^2. Thus:

$$f_2 = -\Delta P \ \pi(x^2 - r^2). \tag{1.19}$$

Finally, the third force, f_3, is the force exerted by the fiber on the left side of the portion of interest. Again, f_3 is a capillary force, so f_3 is proportional to γ and the perimeter of the contour of the drop at the drop extremity, where the drop meets with the fiber so:

$$f_3 = -2\pi r \gamma. \tag{1.20}$$

We want to derive an equation that gives the drop profile, so we need to write our forces as functions of x. Therefore, we need to express $\cos(\theta)$ as a function of x. Using simple trigonometry as shown in the inset in Fig. 1.6, we can write:

$$\cos(\theta) = \frac{dz}{ds} = \frac{dz}{\sqrt{dz^2 + dx^2}} = \frac{1}{\sqrt{1 + \left(\frac{dx}{dz}\right)^2}} = \frac{1}{\sqrt{1 + \dot{x}^2}}, \tag{1.21}$$

where $\frac{dx}{dz}$ is noted $\dot{x}$. We know that the sum of f_1, f_2 and f_3 adds up to zero. So using Eq. 1.18, 1.19, 1.20 we have:

$$f_1 + f_2 + f_3 = 2\pi x\gamma\cos(\theta) - \Delta P\ \pi(x^2 - r^2) - 2\pi r\gamma = 0. \tag{1.22}$$

Substituting Eq. 1.21 in Eq. 1.22 and dividing every term by $2\pi\gamma$ we obtain a differential equation for the drop profile:

$$\frac{x}{\sqrt{1 + \dot{x}^2}} - \frac{\Delta P}{2\gamma}(x^2 - r^2) = r. \tag{1.23}$$

Eq. 1.23 gives us the drop profile $x(z)$ and can also yield the overpressure inside the drop ΔP. We know that Eq. 1.23 holds at the middle of the profile where $x = h$, the maximum height, and therefore where $\dot{x} = 0$. Thus Eq. 1.23 becomes:

$$\frac{\Delta P}{2\gamma}(h^2 - r^2) = h - r, \tag{1.24}$$

which can be easily rewritten as:

$$\Delta P = \frac{2\gamma}{h + r}. \tag{1.25}$$

Eq. 1.25 can be checked for the extreme case where $h >> r$. In this situation, Eq. 1.25 is approximated to $\Delta P = \frac{2\gamma}{h}$, namely the Laplace pressure derived for a drop of radius h.

1.6 Drop on a conical fiber

If the system of a barrel drop on a cylindrical fiber is relatively well understood, the case of a drop on a conical fiber is more complex. The most comprehensive theoretical work on for drop on a conical fiber has been done by Lorenceau and Quéré in 2004 [1]. In section 1.6, we first consider why a drop on a conical fiber spontaneously move towards the thickest end of the fiber. Then we describe Lorenceau and Quéré approach to predict the speed of drops on such fibers. The theory developed by these authors has influenced other authors since [25–27] and is essential to understand the work presented in the present study.

1.6.1 Spontaneous motion of the drop: gradient of Laplace pressure

Even if the spontaneous motion of drops on asymmetric fibers had already been observed, for instance by Carroll in 1989 [28] on mammalian hair displaying a saw profile, Lorenceau and Quéré were the first authors to explain theoretically the driving mechanism for the motion of a drop on a conical fiber [1]. Let's follow Lorenceau and Quéré's explanation and consider a drop on a conical fiber with a gradient of curvature small enough (inferior to 10^{-2}) that it doesn't affect the shape of the drop. Such a drop is shown in Fig. 1.7 (the conicity of the fiber is exagerated to emphasize the difference between conical and cylindrical fibers). The maximum height of the drop h, the drop width w, the drop volume Ω, the horizontal axis or z-axis and the radius of the fiber $r(z)$ are depicted.

With a small gradient of curvature, it is possible to use Eq. 1.25 from Carroll [19] to obtain the Laplace pressure inside the drop. Eq. 1.25 shows that the pressure of the drop depends on the radius of the fiber, which varies with the horizontal coordinate. As ΔP is inversely proportional to r, a drop has a smaller Laplace pressure when the drop is close to the thickest end of the fiber rather than close to the thinner end. Therefore, there is a gradient of Laplace pressure along the fiber, which triggers the spontaneous motion of a drop towards the thickest end.

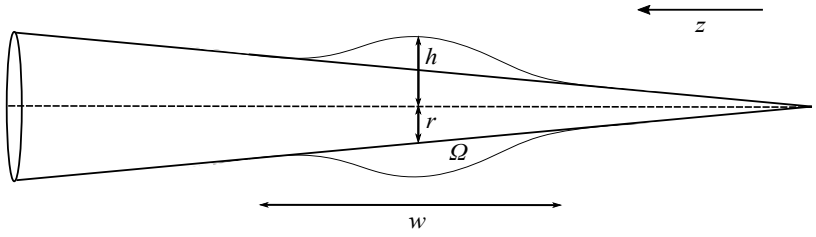

Figure 1.7: Schematic of a barrel-shaped drop on a conical fiber (side view) as studied by Lorenceau and Quéré. Here are displayed the radius r of the fiber at the center of the droplet, the maximum height of the droplet h, the drop width w and the drop volume Ω.

By taking the derivative of ΔP (as defined in Eq. 1.25) with respect to z, the horizontal coordinate of the drop, we can even derive the expression of the gradient of the Laplace pressure at a constant volume:

$$\left.\frac{dP}{dz}\right|_{\Omega} = -\frac{2\gamma}{(h+r)^2}\left(\frac{dr}{dz}+\frac{dh}{dz}\right)_{\Omega}. \tag{1.26}$$

Therefore, it is important to know precisely how the radius of the fiber and also the height of the drop vary with the horizontal position on the fiber. The fiber radius is easy to obtain if there is a control on how the conical fiber is made. In the case where $\frac{dr}{dz}$ it is known, then the only thing we need is how the drop height varies with the fiber radius. The variation can be calculated explicitely using Carroll's theory [1, 19]. However, the approach chosen by Lorenceau and Quéré is to avoid doing the full derivation and instead work in two extreme cases: when $h >> r$ and when $h \approx r$. When $h >> r$, h is considered a constant and doesn't depend on r, so $\frac{dh}{dz} = 0$ and Eq. 1.26 is simplified greatly. The drop is a quasi-spherical drop of constant radius, because the fiber is so small that the fiber almost doesn't influence the liquid shape. Therefore, h scales with $\Omega^{1/3}$. On the other hand, in the case where $h \approx r$, the authors subtitute h by r and Eq. 1.26 is also simplified. The drop is similar to a cylinder and envelops the fiber with a relatively thin liquid film.

1.6.2 Lorenceau and Quéré approach: drop speed prediction

In their work of 2004, Lorenceau and Quéré not only proposed an explanation for the motion of drops on conical fibers, but also suggested a model to predict the speed of such a drop, knowing the different geometrical parameters of the system as well as some fluid characteristics. Even though the authors studied the influence of gravity on the drop, the drop speed prediction model is built for a situation where the fiber is horizontal, which means that gravity doesn't matter. The general assumption behind their drop speed prediction model is that there are only two forces that are applied to the drop: a driving force due to the gradient of Laplace pressure and a force due to viscous dissipation at the contact area between solid and liquid. The inertial terms can be neglected because here $\mathrm{Re} \ll 1$ (see section 1.4.2). Therefore, these forces are equal and it is possible to extract the speed value from the force balance equation.

Driving force

The assumption that is made by the authors for the driving force is that this force is equal to the Laplace pressure gradient (whose expression was given in Eq. 1.26) multiplied by the drop volume Ω. Then, according to what was said in section 1.6.1, this driving force has two possible expressions, depending on the size of the drop. In the case where $h >> r$, then the driving force $f_{driv,sph}$ is:

$$f_{driv,sph} = \left.\frac{dP}{dz}\right|_{\Omega,sph} \Omega = -\alpha \frac{2\gamma}{(h+R_0)^2}\Omega, \tag{1.27}$$

where R_0 is the radius of the quasi-spherical drop and α is the constant radius gradient of the fiber (because in this drop speed prediction model the fiber is perfectly conical, so the radius gradient is considered constant).

On the other hand, in the case where $h \approx r$, the expression of the corresponding driving force $f_{driv,cyl}$ is even simpler since we can replace h by r:

$$f_{driv,cyl} = \left.\frac{dP}{dz}\right|_{\Omega,cyl} \Omega = -\alpha \frac{\gamma}{r^2}\Omega. \tag{1.28}$$

Viscous dissipation

The next step is to evaluate the viscous dissipation inside the drop. The main assumption that is made by the authors is that the dissipation happens mainly at the contact surface between solid and liquid. Therefore, Lorenceau and Quéré approximate the drop as a wedge of width w and of height $h - r$.The wedge approximation is clearly flawed and can only be expected to provide the scaling since the droplet shape is complex. As will be shown in section 3, we find better agreement with the data taking the wedge to be given by w and h. While both approaches provide good agreement with the data, the reason for the better agreement with w and h is not understood at the writing of this thesis. For simplicity here, we will define the wedge in terms of h and w in what follows. Furthermore, because the variation of the shape of the fiber is small on a lengthscale of w, we can approximate the contact surface between the drop and the fiber to a cylinder of height w and of radius r (just as if the conical fiber was locally a cylindrical fiber of an average radius which corresponds to the radius at the middle of the drop). Finally, the wedge has a contact angle θ with the fiber.

To derive the viscous dissipation, one has to integrate the viscous stress over the surface of contact between solid and liquid. Because the drop is axisymmetric, the drop on conical fiber system can be studied entirely in two dimensions, in the plane of x and z coordinates, as they were defined in Fig. 1.6. Here, we changed the definition of x to make x the vertical coordinate of the point of interest inside the drop, not only on the drop contour. The origin of the x-axis is at the crossing point with the z-axis, in the middle of the fiber. Because of the axisymmetry, the viscous forces as they were defined in the Navier-Stokes equations can be simplified as:

$$\eta \nabla^2 \mathbf{v} = \eta \left(\frac{\partial^2}{\partial x^2}, \frac{\partial^2}{\partial z^2} \right) (v_x, v_z), \tag{1.29}$$

where $\mathbf{v} = (v_x, v_z)$ is the speed of a point inside the drop of coordinates (x, z) in the 2D plane defined above.

Because the drop is only moving in the z direction, then we can make the approximation that $v_x = 0$ and we can note $v_z = v$. Furthermore, the most important variation of v happens in the x-direction, so we can neglect the variations along z. Thus, Eq. 1.29 can rewritten as:

$$\eta \nabla^2 \mathbf{v} = \eta \frac{\partial^2 v}{\partial x^2}. \tag{1.30}$$

And finally the viscous stress can be found by integrating Eq. 1.30 with respect to x, so finally the expression for the viscous dissipation, F_η is:

$$F_\eta = \eta \iint_A \left. \frac{\partial v}{\partial x} \right|_{x=0} dA, \tag{1.31}$$

where A is the contact surface and dA a contact surface element, and where the indication $x = 0$ shows that the partial derivative is integrated at the contact line.

The next step is to determine the value of the partial derivative $\frac{\partial v}{\partial x}$. In order to do that, we can integrate two times with respect to x a simplified version of the Navier-Stokes equation applied on a fluid unit inside the drop. In this simplified version of the Navier-Stokes equation, the only terms left are the viscous force and the pressure gradient. The resulting expression obtained for the speed v of this fluid element is:

$$v = -\frac{1}{2\eta} \frac{dP}{dz} x^2 + c_1 x + c_2, \tag{1.32}$$

where c_1 and c_2 are two integration constants. Because we have a no-slip condition, we have $v(0) = 0$ which means that $c_2 = 0$. Also we know that the partial derivative of v with respect to x at $x = h$ is equal to zero, because the speed reaches its maximum at the top of the drop. Thus, we can obtain the value of c_1 and the full expression of v is:

$$v = \frac{1}{\eta}\frac{dP}{dz}\left(hx - \frac{x^2}{2}\right). \tag{1.33}$$

Consequently, we can obtain the partial derivative of v with respect to x at $x = 0$, just by taking the derivative v given in Eq. 1.33 and replacing x by 0:

$$\left.\frac{\partial v}{\partial x}\right|_{x=0} = \frac{1}{\eta}\frac{dP}{dz}h. \tag{1.34}$$

We still have to replace the pressure gradient $\frac{dP}{dz}$ by the quantity of interest, the average speed of the drop, $\overline{v}$. Therefore, the next step is to derive $\overline{v}$ by integrating the expression of v given in Eq. 1.33 over the full height of the drop:

$$\overline{v} = \frac{1}{h}\int_0^h \frac{1}{\eta}\frac{dP}{dz}\left(hx - \frac{x^2}{2}\right)dx = \frac{1}{3\eta}\frac{dP}{dz}h^2. \tag{1.35}$$

Rearranging Eq. 1.34 with the result of Eq. 1.35, we finally obtain:

$$\left.\frac{\partial v}{\partial x}\right|_{x=0} = \frac{3\overline{v}}{h}. \tag{1.36}$$

With Eq. 1.35, we can fully derive the viscous dissipation as defined in Eq. 1.31. The integral over the surface of contact A is an integral with respect to two variables: z which varies from 0 to w (element of integration dz) and over the perimeter of the cross-section of the fiber (element of integration $rd\phi$ with ϕ the position angle varying from 0 to 2π). Because there is no dependancy in ϕ in the integral, we can replace the integration by multiplying the whole expression by a factor of $2\pi r$. Furthermore, the integral with respect to z can be separated into two identical integrals: one from 0 to $w/2$ and the other from $w/2$ to w. Instead of calculating both, only one integral is kept and a factor of 2 is added in front of the expression. Therefore, we have the following expression:

$$F_\eta = 4\pi r\eta \int_{w/2}^{w} \frac{3\overline{v}}{h} dz. \tag{1.37}$$

Using simple trigonometry, we can express h as a function of the contact angle θ and z the horizontal coordinate:

$$h = z\tan(\theta). \tag{1.38}$$

If we consider the wedge geometry, then $z = w/2$ and the integral in Eq. 1.37 is equal to one. If we keep the general case and we replace h by its value in Eq. 1.38, we have:

$$F_\eta = \frac{12\pi r\eta\overline{v}}{\tan(\theta)} \int_{w/2}^{w} \frac{dz}{z}. \tag{1.39}$$

The last integral in Eq. 1.39 is a constant that we can call l, the logarithmic factor. So the final expression for F_η is:

$$F_\eta = \frac{12\pi r\eta\overline{v}l}{\tan(\theta)} \propto \frac{r\eta\overline{v}l}{\tan(\theta)}, \tag{1.40}$$

where one can replace $\tan(\theta)$ by θ if the conditions are such that the contact angle remains small. The only parameter left to determine is the angle θ. Lorenceau and Quéré suggest that the viscous dissipation is global and in the case of a global dissipation, θ is expressed using the wedge. If we use the wedge as defined by Lorenceau and Quéré (the wedge height is $h - r$ and the width is w) and simple trigonometry:

$$\tan(\theta) = \frac{2(h-r)}{w} \propto \frac{h-r}{w}. \tag{1.41}$$

Otherwise, if we use the wedge approximation that we suggested, where the wedge height is h and the width is w, the expression obtained for $\tan(\theta)$ is similar to Eq. 1.41. The only difference is that $h - r$ would be replaced by h. To stay as close as possible

to the theory Lorenceau and Quéré proposed, we will keep their wedge approximation to write the final expressions of the drop speed.

Speed prediction

As described at the begining of section 1.6.2, the sum of the two forces, the driving force and the viscous dissipation, is equal to zero:

$$F_{driv} + F_{\eta} = 0, \tag{1.42}$$

because these forces are the only two relevant forces in the drop speed prediction model and that the inertia terms are negligible. Consequently, we have two equations for $\overline{v}$, because the expression of F_{driv} depends on the relative size of the drop. For a quasi-spherical drop and a quasi-cylindrical drop, we have respectively:

$$\overline{v}_{sph} = \frac{2\gamma}{\eta l}\left(\frac{h-r}{w}\right)\left(\frac{\Omega}{r(h+R_0)^2}\right)\alpha, \tag{1.43}$$

and

$$\overline{v}_{cyl} = \frac{\gamma}{\eta l}\left(\frac{h-r}{w}\right)\left(\frac{\Omega}{r^3}\right)\alpha. \tag{1.44}$$

In theory, this drop speed prediction model allows us to fully predict the speed of a drop on a conical fiber, knowing the viscosity and the surface tension of the fluid, as well as the geometrical parameters of the system. In their paper, Lorenceau and Quéré only present data corresponding to small cylindrical drops.

Chapter 2

Experimental Methods

2.1 Conical fiber preparation

The conical glass fibers are all produced using standard borosilicate glass capillary tubes that have an inner diameter of 0.7 mm and an outer diameter of 1 mm (World Precision Instruments Inc., 1B100-6). Glass was chosen because of its smooth and controlled surface. Glass has a zero contact angle with silicone oil.

2.1.1 Cleaning and pulling process of the conical fiber

Before any experiment, these capillary tubes are cleaned with acetone and then methanol, in order to remove dust and other particles.

After the cleaning step, these capillary tubes are transformed into conical fibers or micropipettes by stretching the glass with a magnetic pipette puller (Narishige, PN-30). With the pipette puller, the tube is heated by a hot filament, while one side of the tube is pulled by a magnet and the other side of the tube is held in place by a tightened screw. Once the glass starts to melt, the magnetic attraction takes over and the glass is streched. This stretched part of the tube is conical and both its radius and its radius gradient are varying. The extremity of the tube is also much thinner, with a diameter on the order of the tens of microns. The thinnest part of the micropipette is flexible and bends under its own weight. Because we need the fiber to be rigid, the extremity of the fiber is removed by cutting it with tweezers. As

the cutting process creates glass particles, we then blow compressed nitrogen gas on the fiber to remove the particles. In the end, the conical part of the fiber has a total length of 1-2 cm and the diameter of the extremity is typically around a hundred of microns or a little less. We observe that the shape of every micropipette is unique, with its own radius and gradient profiles.

We briefly considered coating the surface of the micropipette with a polymer thin film (e.g. polystyrene), in order to improve the micropipette surface smoothness. However, after an observation of the coated surface under the optical microscope and the Atomic Force Microscope (AFM), we concluded that the coating didn't bring any significant improvement and decided to keep the surface of the micropipettes non-coated.

2.1.2 Auxiliary capillary tubes

Two more types of capillary tubes are also prepared for our experimental set-up, that we call auxiliary or intermediate pipettes. The first auxiliary pipette is just a cylindrical glass capillary tube, that is cleaned as described in section 2.1.1. The auxiliary tube is dipped in the liquid that we want to use for the drop and placed in a holder with a large drop sitting on its tip. The auxiliary tube acts as a reservoir of this liquid for the rest of the experiment. The second auxiliary pipette is cleaned and pulled with the same methods given in section 2.1.1. However, the conical part of the second auxiliary pipette is usually cut less short (around 2-4 cm) than the conical fiber of interest, because we want the drop to prefer to go on the fiber of interest. The reason for a droplet to spontaneously transfer from the thinner to the thicker pipette is that the droplet has a larger surface area in contact with glass on a thicker pipette and that it is more energetically favorable for the silicone oil to wet the glass substrate and thus have the largest contact surface with the substrate (see section 1.3). The second auxiliary pipette acts as the intermediate between the reservoir and the conical fiber: the second auxiliary pipette is used to transfer a small drop from the reservoir to the conical fiber. The full process is presented in section 2.2.2.

2.2 Experimental set-up

2.2.1 Liquid used for the droplets

The liquid that is used to make droplets has to satisfy some conditions: having a known and controlled viscosity, being chemically stable and non-volatile. In order to make measurements easier, the liquid needs to have a high viscosity. The droplet speed is lowered when the viscosity is higher and thus the image recording is made easier. Therefore, doing measurements with water was not an option given water volatile nature, even if water is the actual liquid migrating on cactus spines. Preliminary measurements were done with glycerol. However, during a set of experiments, the viscosity of glycerol would change from one droplet to another. In fact, glycerol is hygroscopic, which means that glycerol tends to absorb the moisture in the air. Consequently, the added amount of water lowers its viscosity. The changes in viscosity are especially important in our case, where the volumes are small and where the fiber is covered by a glycerol thin film, which has a huge surface area and is particularly sensitive to the moisture.

Therefore, we chose to use several silicone oils, i.e. polydimethylsiloxanes (PDMS), as the drop liquid. As mentioned earlier, silicone oils have a zero equilibrium contact angle with glass. Silicone oils also are chemically stable even for long periods of time and have tunable viscosities. Three types of silicone oil were used in our experiment: vinyl terminated polydimethylsiloxane, silanol terminated polydimethylsiloxane, and vinyl terminated (0.3-0.4 % vinylmethylsiloxane) dimethylsiloxane copolymer (Gelest). These silicone oils have kinematic viscosities of 5000 cSt, 2000 cSt and 1000 cSt respectively and all these silicone oils have the same surface tension, which is 22 mN/m.

2.2.2 Droplet brushing

The first step of the experimental process is to bring small droplets with volumes ranging from $5 \cdot 10^{-2}$ to $20 \cdot 10^{-2}$ mm^3 on the tip of the conical fiber. The auxiliary micropipettes described in section 2.1.2 are used. The intermediate conical fiber is brought in contact with the drop sitting on the tip of the liquid reservoir capillary

tube. The tip of this intermediate fiber is dipped inside this drop and withdrawn slowly, depositing small droplets on the tip. The intermediate pipette is needed because there are several droplets (and a thin film of liquid enveloping the fiber) at the same time, with the dipping and withdrawing technique. We cannot make a reproducible measurement with several droplets. In fact, we find that the presence of droplets nearby the droplet of interest influenced the speed of this droplet of interest, which is why the results lack reproducibility.Once at least one droplet of the desired size is on the intermediate pipette, the extremity of the intermediate pipette is brought perpendicularly close to the conical fiber of interest, as depicted in Fig. 2.1.

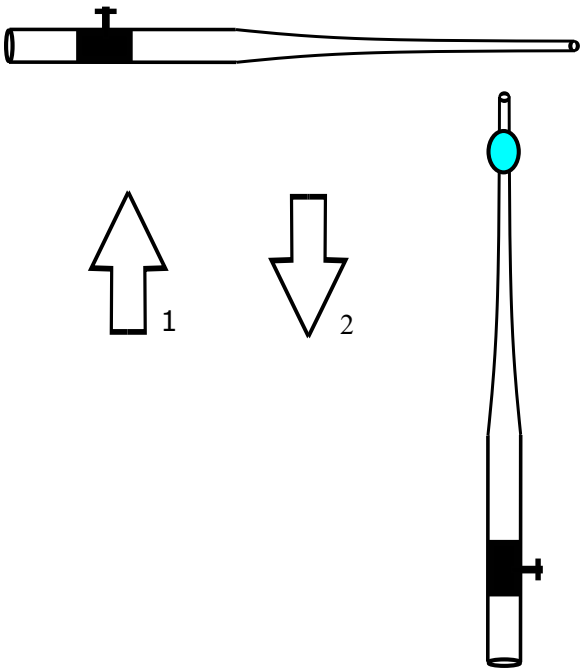

Figure 2.1: A top view schematic illustrating the process used to place the droplet on the conical region of the fiber of interest (horizontal fiber). An intermediate pipette (vertical one on the schematic) is used to brush droplets of liquid on the pipette of interest along the directions highlighted by the arrows. The holders that maintain both pipettes are depicted in black. 1 is the approach step where the intermediate pipette is brought on top of the pipette of interest. 2 is the brushing step, where is the droplet on the intermediate pipette is gently transfered to the pipette of interest. Initially, that droplet was put on the intermediate pipette by dipping the intermediate pipette into a liquid reservoir (typically a drop at the end of a thick pipette).

First, the intermediate pipette is brought on top of the fiber of interest, following the direction of the arrow 1 in Fig. 2.1. The droplet is now in contact with both pipettes. Second, the intermediate pipette is slowly withdrawn in the direction shown by arrow 2, brushing the droplet on the conical fiber. The process is made easier in the case where the intermediate pipette is thinner than the pipette of interest, as the droplet will be more stable if it takes a barrel shape around a thicker fiber 1.6.1. Once the droplet is detached from the intermediate pipette, that the intermediate pipette is removed and that the droplet has taken a stable barrel shape on the fiber of interest, we can start recording a movie of the droplet motion.

At first, a more direct method was used to bring droplets on conical fibers. The fiber of interest itself was brought at the surface of the reservoir drop and thanks to capillarity, the liquid started penetrating inside of the fiber. The other side of the fiber was connected to a syringe through some tubing. The syringe could help pull some liquid in the fiber. More importantly, the syringe was used to eject droplets from the conical fiber, that would then move to the exterior of the pipette, become barrel-shaped droplets and start migrating towards the thickest end of the fiber. This droplet ejection method is similar to the method used by Li and Thoroddsen [25]. Even if the direct method was simpler, a significative variability of droplet speed was observed because of the interaction of the droplet either with satellite droplets left behind during the ejection or with the liquid left inside the pipette. For this reason, we decided to bring the droplets perpendicularly with an intermediate pipette.

2.2.3 Global set-up and image recording

The experimental set-up for image recording is depicted in Fig. 2.2.
The pipette of interest is held in place horizontally with a holder on the cylindrical part of the pipette. This holder is itself fixed on a horizontal plane. Therefore, gravity doesn't play a role in the motion of the droplet. To check the assumption of negligible gravity even further, the full set-up, including the conical fiber and the microscope, was tilted at an angle (approximately 20°). Measurements were done in with the tilted angle and no difference was found between the configuration where the set-up is tilted and the configuration where the set-up is horizontal, confirming that we can

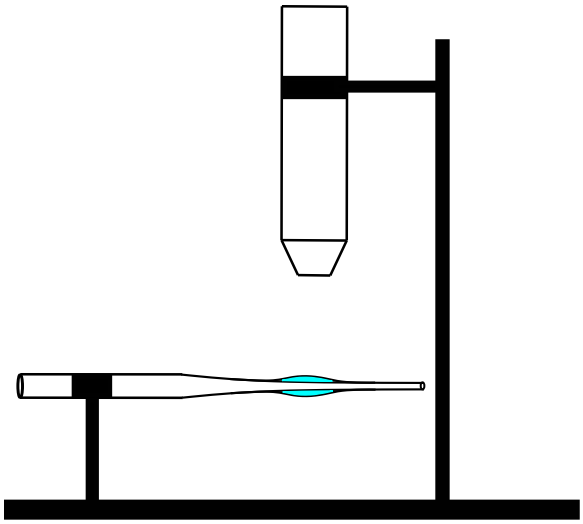

Figure 2.2: A schematic presenting the main elements of the experimental set-up from a side view. A pipette holder maintains a conical pipette in the field of view of the camera. The pipette itself is fixed to be horizontal and a droplet is brought on its conical region using a intermediate pipette as shown in Fig. 2.1. The camera is connected to a microspcope objective and is fixed on top of the pipette by a post and a holder.

neglect the effect of gravity.

On the same horizontal plane, there is also a post which holds a CMOS camera (Thorlabs, DCC1240M) combined with a 2.5x objective. The assembly of both works as an optical microscope. The camera and the objective are positioned on top of the region of interest of the micropipette. The field of view is 5.5 mm long and 2 mm wide, while the droplets have characteristic sizes on the order of 500 μm. The microscope is connected to a computer where the images of the droplet are recorded, using the open source Micro-manager software. The images were usually taken at a rate of one image per second (the rate was adapted to the actual speed of the droplet, to obtain more accurate measurements). Typical images can be seen with the results in section 3.2. Recordings start as soon as the droplet reaches a stable barrel shape and are stopped either when the droplet looses its barrel shape or axial symmetry or when the droplet exits the field of view. The droplet usually looses its barrel shape when the size of the droplet becomes too small compared to the radius of the fiber,

or more rarely because of an irregularity on the fiber surface (e.g. a dust particle).

When a first droplet is brought on a conical fiber and starts moving spontaneously towards the thickest end of the fiber, the droplet leaves behind a thin film of liquid that coats the fiber surface. The measurements that are recorded for the purpose of the present work have to be made on a homogeneous thin precursor film. Otherwise, the symmetry between the front and the rear of the droplet is broken and simplifying symetry assumptions are no longer valid (see assumptions in [1] and section 3.2). Therefore, the motion of the first two droplets that migrates on the fiber isn't analysed. Data acquisition starts with a third droplet, when the film is considered homogeneous enough for the droplet to be laterally symmetric. The motion of droplets of different volumes are then recorded on the same pipette. Later, more droplets are brought to different pipettes of varying sizes and gradients profiles. We also repeat our measurements with silicone oils of different viscosities.

2.3 Data analysis

Once movies of droplets migrations are recorded, the next step is to analyse the movies to extract all the relevant parameters for our model. The analysis was performed using Matlab (2016 version) and is described in section 2.3.

2.3.1 Droplet and fiber edge detection

To obtain most of the relevant parameters, we need to track precisely the droplet on every image. We wrote a Matlab script, which detects the edge of the droplet and the edge of the fiber for every image. The first step of this script consists of taking an image of the region of the fiber on which droplets will migrate, before bringing any droplet to the fiber. The image is used to obtain a reference image for the shape of the fiber. The script analyses the intensity of the pixels in the image. There is an approximately linear transition in the intensity of the pixels between the background and the fiber. If we fit the pixel intensity transition with a linear trendline and take the middle of the trendline, we obtain the boundary between background and fiber. Using this reference image displaying the fiber only and the corresponding profile, we

have the radius of the fiber for every horizontal position. By taking the derivative of the radius with respect to the horizontal position, we obtain the radius gradient.

The second step of the script is to use the same type of boundary detection process but for the first image with a droplet on the fiber. Similarly, the script determines the boundary of the droplet and fiber combined. The resulting boundaries are shown in Fig. 2.3 (1): the upper boundary is drawn in blue and the lower boundary in orange, on top of the droplet and fiber picture.

The next step is then to subtract the profile of the fiber alone obtained in the first step, from the profile of the drop and fiber combination. The resulting profile is the profile of the drop only, centered vertically on zero. The profile is displayed in Fig. 2.3 (2a) and also in Fig. 2.3 (2b), which is zoomed in on the droplet shape. The color code for the upper and lower boundaries is the same as in Fig. 2.3 (1). The maximum amplitude of the profile of the upper boundary approximately indicates the center of the drop and hence the droplet horizontal position. However, because our image has a limited precision (the smallest unit is one pixel), there is noise in the profile. Thus, we fit the top of the drop upper boundary to a parabola. The maximum given by the equation of the parabola is a more exact sub-pixel maximum and the coordinates of the maximum give us the horizontal position of the droplet. We also fit a parabola to the lower boundary profile and determine the corresponding horizontal position. Both parabolas are shown in Fig. 2.3 (2a) and (2b): the upper parabola is purple and the lower parabola is yellow. The final horizontal position for the droplet is the average of both values.

Once the position of the droplet was determined for the first image, the same operation can be repeated several times for following images showing the droplet migration. A superimposition of the resulting profiles with their corresponding parabolas is displayed in Fig. 2.3 (2a). We have the position of the droplet at all times and therefore, by taking the derivative of the position, we also have its average speed.

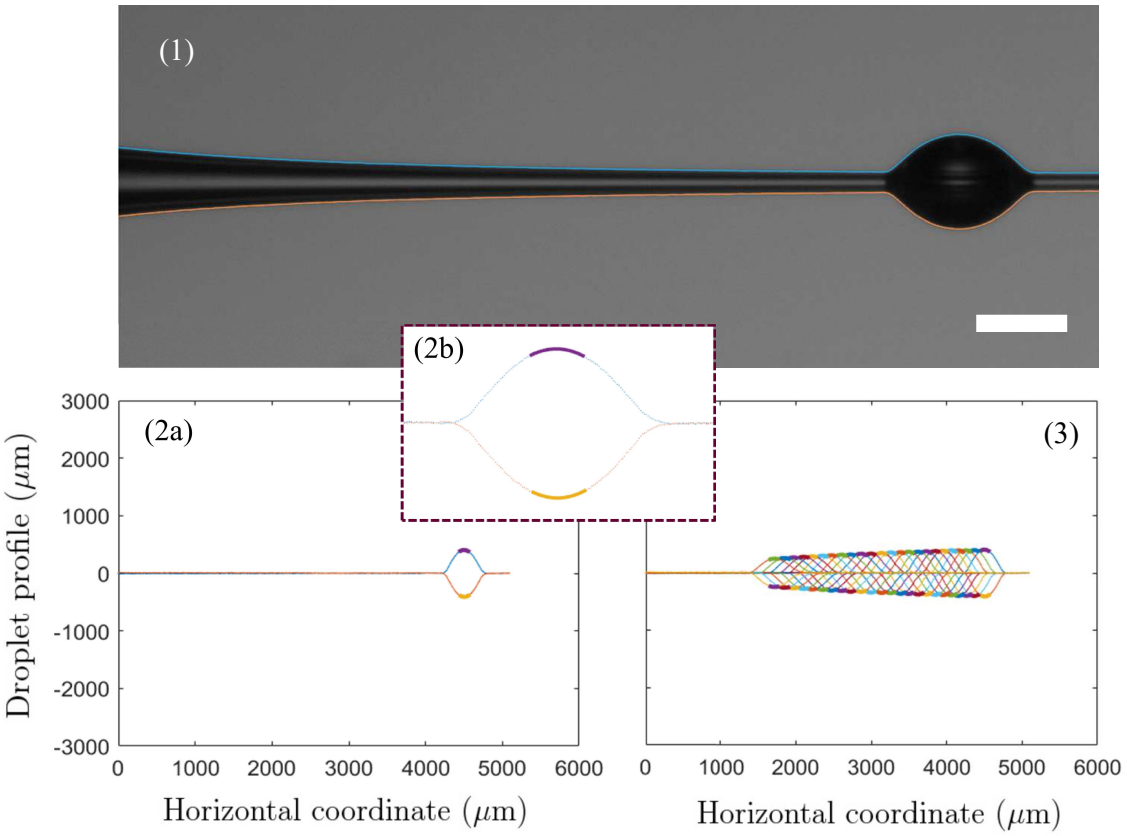

Figure 2.3: (1) An image of a silicone oil droplet on a conical glass fiber. The scale bar represents 500 μm. Using Matlab to perform boundary detection, the top edge of the system fiber and droplet is detected and drawn in blue, the bottom edge is drawn in orange. (2a) The profile of the fiber is subtracted to the top and bottom edges drawn in (1), giving the graph of the profile of the droplet itself centered on 0 vertically, as a function of the horizontal coordinate. Both the top and bottom resulting profiles are fitted by a parabola around their respective maximum and minimum height (purple and dark yellow curves respectively). (2b) This image is a detail of the graph (2a), zoomed in on the droplet itself. (3) Graph showing a superimposition of all the profiles of the droplet shown in (1) and (2) at subsequent times.

2.3.2 Extraction of the relevant parameters

With a precise detection of the droplet shape, we have seen that we can obtain the droplet position and the droplet average speed. We can also measure the droplet height, h, as defined in section 1.5.2, by taking the maximum of the parabola and adding to that the radius of the pipette at that point. The droplet width w is extracted

by determining the width of the non-zero part of the profile shown in Fig. 2.3 (2a) and (2b). Here, non-zero corresponds to the droplet profile exceeding the radius of the fiber by a threshold corresponding to approximately 2 μm or 5% of the smallest radius of the pipette. Finally, the droplet volume Ω can be derived by integrating the boundary profile around the fiber. Therefore, we have all the parameters needed to test models for droplet speed prediction.

Chapter 3

Results

In section 3.1, the reader will find a short introduction to the paper draft resulting from my master's project, in which my role and the role of the other collaborators are described. Then section 3.2 presents a manuscript of this paper draft.

3.1 Presentation of the paper

Droplet migration on conical glass fibers

C. Fournier, R.D. Schulman, É. Raphaël and K. Dalnoki-Veress (2018).

In this work, we investigate the spontaneous migration of droplets on a conical fiber and propose a model to predict the droplets speeds. We present our experimental set-up in which the conical fibers are pulled glass capillary tubes and the droplet liquids are different types of silicone oils of known viscosities. The droplet motion is captured with optical microscopy, using the combination of a CMOS camera and a 2.5x objective. The resulting movies are analysed using a Matlab script. The script tracks the position of the droplet by detecting the droplet edges at all time. Thus, the script extracts the droplet speed and all the other geometrical parameters of the droplet on conical fiber system: the height, width and volume of the droplet and the radius and radius gradient of the fiber.

We then propose a simple theoretical model to predict the droplet speed as a function of the geometrical parameters of the droplet on conical fiber system and the liquid characteristics (viscosity and surface tension). In our model, gravity is negligible because the droplets characteristic sizes are less than κ^{-1}. Therefore, the only two forces at play are the driving force created by surface tension and the viscous dissipation at the contact line between the droplet and the fiber. Furthermore, the inertial terms can also be neglected ($\mathrm{Re} \ll 1$), consequently both forces are equal. The resulting equation predicts the droplet speed, as the viscous dissipation depends directly on it. The model matches our experimental data well and works for a large range of droplet volumes, different conical fibers (various radius and radius gradients) and 3 different silicone oils with viscosities of 1000 cSt, 2000 cSt and 5000 cSt.

In this study, the experimental set-up was built with the help of Rafael Schulman and Kari Dalnoki-Veress. The experiments, the creation of a Matlab script for image analysis and the data analysis itself were performed by me. A theoretical model for the droplet speed prediction was developed in collaboration with Rafael Schulman, Kari Dalnoki-Veress and Élie Raphaël. I wrote this draft, which was edited by Rafael Schulman and Kari Dalnoki-Veress.

3.2 The paper

The paper *Droplet migration on conical glass fibers* can be found on the next page.

Droplet Migration on Conical Glass Fibers

Clementine Fournier,[1] Rafael D. Schulman,[1] Élie Raphaël,[2] and Kari Dalnoki-Veress[1, 2, *]

[1] *Department of Physics and Astronomy, McMaster University, 1280 Main St. W, Hamilton, ON, L8S 4M1, Canada.*

[2] *Laboratoire de Physico-Chimie Théorique, UMR CNRS Gulliver 7083, ESPCI Paris, PSL Research University, 75005 Paris, France.*

(Dated: August 11, 2018)

The spontaneous migration of droplets on conical fibers is studied experimentally by depositing silicon oil droplets onto conical glass fibers. Their motion is recorded using optical microspcopy and analysed to extract the relevant geometrical parameters of the system. The speed of the droplet can be predicted as a function of these parameters and the fluid properties using a simple theoretical model, which balances viscous dissipation against the surface tension driving force. The experimental data are found to be in good agreement with the model.

I. INTRODUCTION

Spontaneous water transport systems at small lengthscales are a crucial feature for the survival of many living organisms and have been widely studied. In some cases, the aim is to remove excess water. For instance, water striders' legs [1] and birds' feathers [2] have water repelling properties. However, most of the living systems employing water transport do so for harvesting purposes. Spider webs [3], desert beetles' backs [4], desert moss structures [5] and cacti spines [6–8] help these plants and insects catch the water necessary for their survival. In the case of cacti, the water system is based on a simple mechanism: when fog condenses at the tip of a cactus spine, which is in fact a conical fiber, it forms droplets that spontaneously migrate towards the largest end of the spine under the action of surface tension as a driving force. Many recent artificial water harvesting systems have been inspired by this mechanism [9–13], with the intent of fighting drought in arid areas. However, there are still unanswered questions about the droplet dynamics in this system.

A standard framework to describe droplets on cylindrical fibers has been developed by Caroll [14, 15], who also highlighted the existence and the transition between two possible configurations for a droplet on a fiber: the clam shell configuration, in which the droplet is only on one side of the fiber, and the barrel configuration, in which the droplet is axisymmetric and envelopes the fiber. Using the theory developed by Caroll, the work of Lorenceau and Quéré [16] was the first one to propose a theoretical model to explain barrel shaped droplet dynamics on conical fibers. They showed that droplet motion originates from the presence of a gradient in Laplace pressure along the fiber: the thicker the fiber is, the smaller the Laplace pressure will be, thus creating a spontaneous migration of the droplet towards thicker regions of the fiber. Their work is focused on large drop on fiber systems (characteristic length scale of approximately 1 mm), at which gravity must be taken into account and for a small range of relative drop sizes, i.e. the drop size compared to the fiber radius. The experimental results of Lorenceau and Quéré focus on the case where the drop size is comparable to the fiber radius and therefore, the drop is quasi cylindrical. Other recent theoretical, simulation and experimental works on this topic [17–20] have focused on large length scales, and in some of these studies, investigated where gravity fully balances the surface tension driving force. Smaller length scales have been explored in a more recent study, where the data was analysed with the model presented by Lorenceau and Quéré [21]. Moreover, the migration of clam shell drops was investigated [22]. It is relevant to note that the spontaneous migration of drops inside a conical tube or a wedge has been studied recently and theoretical models were proposed to describe it [18, 23–28]. Even if the geometry differs, the same forces matter, like gravity or the force applied by a gradient of Laplace pressure. More generally, the assymmetry created by cone-like structures has been an inspiration in this field, for instance in elastocapillarity, where a liquid drop between two elastic fibers or thin sheets can make them coalesce or separate [29–33].

In the present work, we study the migration of highly viscous, totally wetting, and thus barrel-shaped, droplets on conical glass fibers on length scales at which gravity can be neglected. We explore a large range of drop sizes relative to the fiber radius. In this droplet on conical fiber system, the only forces acting on the droplet are a driving force

* dalnoki@mcmaster.ca

originating from surface tension and the viscous shear force. We develop a simple theoretical model, which though different to that of Lorenceau and Quéré, has similar ingredients, to predict the droplet speed as a function of the radius, radius gradient of the fiber, droplet volume, as well as the surface tension and viscosity of the fluid.

II. EXPERIMENTAL SET-UP

The glass fibers were prepared by pulling standard borosilicate glass capillary tubes with an outer diameter of 1 mm in a magnetic micropipette puller (Narishige PN-30). The resulting shape of the transformed pipette was a nearly conical fiber of changing diameter (with a tip size of tens of microns) and gradient. The variations of diameter and gradient were unique to each pipette. Glass was chosen because it presents a well controlled and smooth surface. Three different silicon oils, i.e. polydimethylsiloxanes (PDMS), were used: vinyl terminated polydimethylsiloxane, silanol terminated polydimethylsiloxane, and vinyl terminated (0.3-0.4 % vinylmethylsiloxane) dimethylsiloxane copolymer (Gelest). Their respective kinematic viscosities are 5000 cSt, 2000 cSt and 1000 cSt and have a surface tension of $\gamma = 22$ mN/m. Silicon oils were the most appropriate liquids in this case, as they have well controlled viscosities, are non-volatile, and chemically stable. These oils also totally wet glass which means that droplets have a zero equilibrium contact angle with the fibers.

Initially, a given glass fiber is cleaned using acetone and methanol to remove all potential dust particles. It is then fixed in a horizontal orientation and a small droplet of PDMS is placed close to the tip as shown in Fig. 1(a) at $t = 0$ s. The droplet is positioned there using an intermediate micropipette that brushes it perpendicularly on the top of the fiber. Once the droplet is deposited, its motion is recorded in top view using an optical microscope as shown in Fig. 1(a). An average frame rate of 1 image per second is used. The recording goes on until either the droplet exits the field of view or it loses its barrel shape and axial symmetry, which happens when the fiber radius becomes too large compared to the droplet volume. The first two droplets migrating on the fiber coat it with a thin film of PDMS. The data for these first two droplets are not analysed, as we wish to study droplet motion on fibers which are pre-wet by a homogenous thin liquid film. Subsequently, the migration of several droplets of different volumes are recorded and analysed.

To make sure that gravity had no impact on the measurements, the experimental set-up (including the conical fiber and the microscope) was tilted at an angle and the experiment was reproduced in this configuration. The resulting data presented no difference with the rest of the recorded data, thus gravitational effects are overwhelmed by surface tension driven forces.

Several parameters of interest are extracted from the recordings: the fiber radius r and radius gradient $\frac{dr}{dz}$ as a function of the axial coordinate z, as well as the height of the droplet h, its volume Ω, width w, and position at all times. Some of these parameters are denoted in Fig. 1(b). All of them are obtained by direct image analysis. The droplet position is retrieved by averaging the z-position of the maximum and minimum of parabolas fitted respectively to the top and bottom of the detected edge of the droplet. The speed v is calculated as the derivative of the resulting position.

As the goal of this study is to find a comprehensive expression for v as a function of all the other variables, a first step is to look at how the speed varies with the other parameters of the system. A plot of v as a function of the droplet position (Fig. 2) shows the speed of four droplets of different volumes that migrated on the same pipette. From this plot, it is evident that the speed increases with position. However, we also know that both the radius and the gradient of the fiber increase with position. Therefore, the raw data does not allow us to dissociate the effect of each parameter. A second observation is that the speed increases with the droplet volume. Since there are several variables which influence the droplet speed, it is necessary to develop a model in order to attain a comprehensive expression for v as a function of all the relevant parameters of the system.

III. MODEL

In order to develop a model, we consider all the forces applied on the droplet. A first assumption is that gravity is negligible as we are well below the capillary length, calculated to be $\sim$1 mm. As described earlier, this assumption has been experimentally validated. We also assume that inertial forces are negligible, as the Reynolds number is on the order of 10^{-6}. Two main contributions remain: the driving force caused by the surface tension γ between the air and the silicone oil, as depicted in Fig. 1(b), and the viscous dissipation in the liquid. The first contribution,

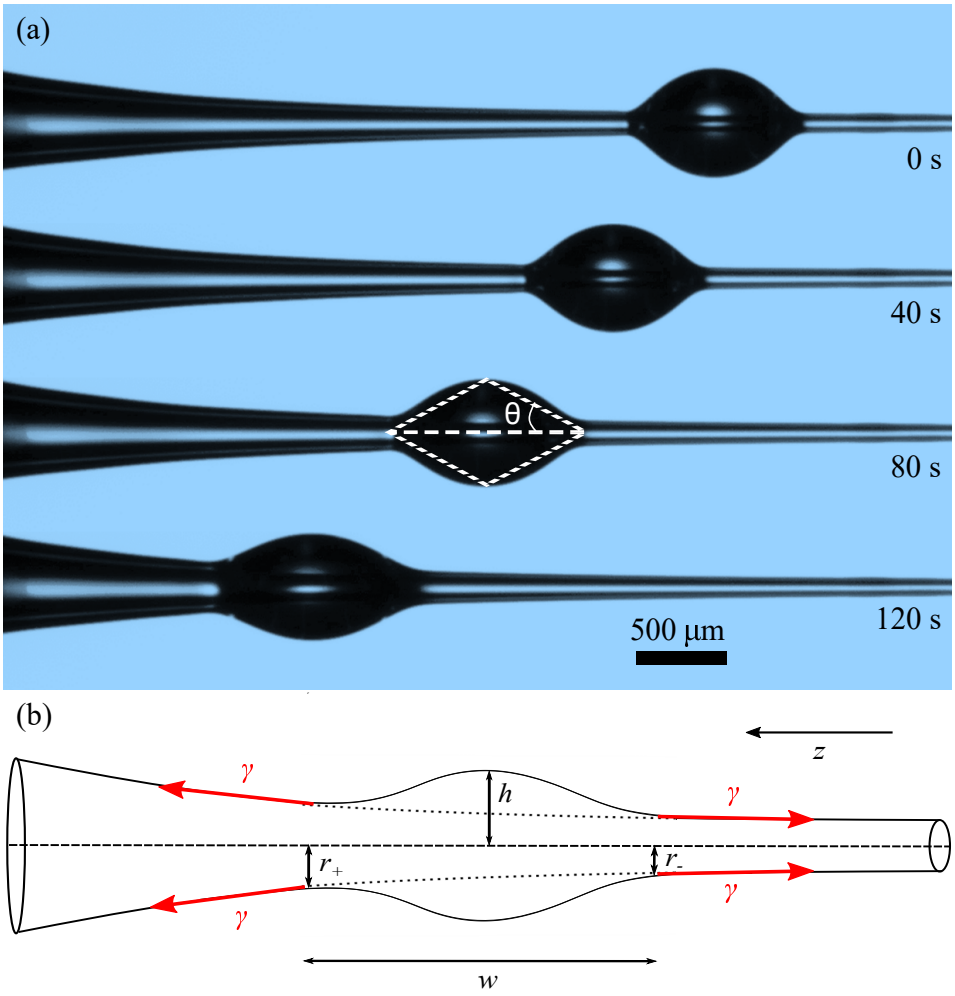

FIG. 1. (a) Microscope images of the top view of a droplet migrating along a conical fiber at different times with the wedges mentionned in the model section drawn on the third panel. (b) Schematic of a barrel-shaped droplet on a pre-wetted conical fiber with the relevant lengths identified. The surface tension γ acting as a driving force on the droplet is also shown.

which we denote F_γ, is the net surface tension force exerted by liquid-air interface of the pre-wetted fiber onto the droplet volume. It is composed of a difference between two surface tension forces: one acting at the extremity of the advancing side where $r = r_+$, and another acting at the receding side where $r = r_-$. A simple approximation gives the following final expression for F_γ:

$$F_\gamma \sim 2\pi\gamma r_+ - 2\pi\gamma r_- \sim \gamma w \frac{dr}{dz}. \tag{1}$$

The second contribution, denoted F_η, results from the viscous force at the solid-liquid interface. In order to attain a simple expression for this quantity, we approximate the droplet shape as two joined wedges drawn in the third panel of Fig. 1(a). Although a crude approximation, it should suffice for quantifying the dissipation at the level of scaling. In this case, the viscous force can be evaluated by integrating the shear force over the entire liquid-solid area ($A_{\rm ls}$) beneath the wedge [34]:

$$F_\eta \sim \iint_{A_{\rm ls}} \eta \frac{dv}{dy}\bigg|_{y=0} \sim \frac{\eta r v}{\tan(\theta)}, \tag{2}$$

where y represents the radial coordinate, which is equal to 0 when the point of interest is at the center of the fiber and θ is angle of the wedges which approximate the droplet. Here, we have neglected any prefactors and the logarithmic term which truncates the integral in viscous wedge dissipation (see Ref. [34]). The only parameter from this expression

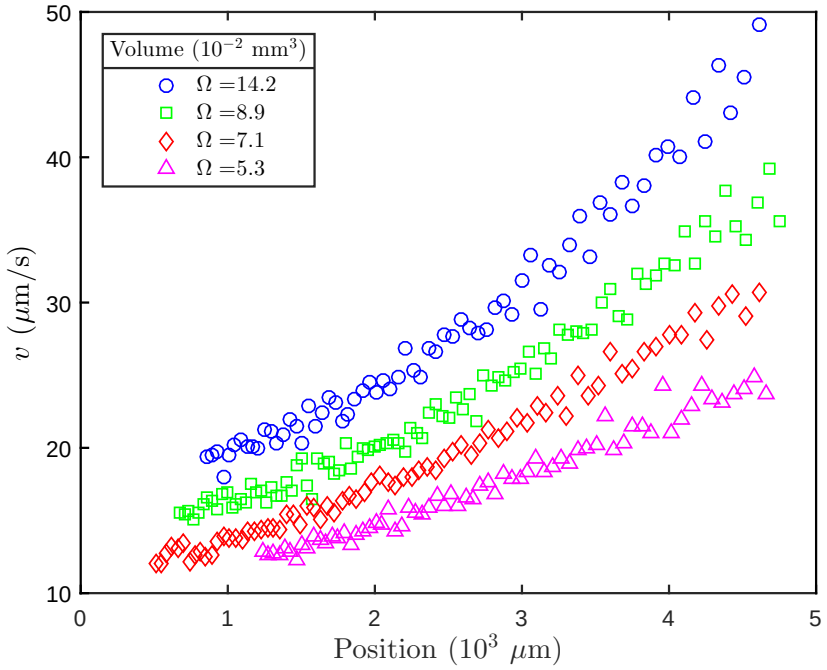

FIG. 2. The speed of several droplets migrating one after another along the same conical fiber plotted as a function of their position on the fiber. The different markers represent different volumes.

that has not directly been measured in the experiment is $\tan(\theta)$. Using simple trigonometry, we find:

$$\tan(\theta) = \frac{2h}{w}\,. \tag{3}$$

Substituting Eq. 3 back into Eq. 2, a final expression for F_η is obtained:

$$F_\eta \sim \frac{\eta r v w}{h}\,. \tag{4}$$

In the absence of gravity and inertia, we must have $F_\eta \sim F_\gamma$. Thus, equating Eq. 1 and Eq. 4 yields an expression for the speed as a function of all the other relevant parameters:

$$v \sim \frac{\gamma}{\eta}\frac{h}{r}\frac{dr}{dz}\,. \tag{5}$$

These parameters can all be fixed externally except for h, as η and γ are fluid properties and r and $\frac{dr}{dz}$ both are geometrical properties of the fiber which can be fixed with the appropriate experimental methods [16, 21]. However, h must be measured *in situ*. The droplet height can be predicted with an exact equation of the shape of a droplet on a fiber. In fact, this has been studied previously in the case of a cylindrical fiber, where it has been shown that there is a non-trivial dependence on the fiber radius [14, 15, 35, 36]. The derived relationship between h and r according to the theory is plotted as a solid black line in Fig. 3. This plot is drawn with reduced coordinates, i.e. $h/\Omega^{1/3}$ and $r/\Omega^{1/3}$.

The dashed black line represents the asymptotic regime in which $h = r$. For large r, h tends towards r and the droplet become quasi-cylindrical and takes the shape of a cylinder enveloping the fiber. Our experimental data is also plotted in Fig. 3, with markers of three different colors, corresponding to the three different viscosities we tried: 1000 cSt (red), 2000 cSt (green) and 5000 cSt (blue). The experimental data matches the theoretical master curve and is also in a region of the curve where h stays approximately constant over one migration of a droplet on a given fiber (variation of less than 5%). We also see that h is close to the h of a droplet in a quasi-spherical regime, where r tends towards 0 and where the volume of a droplet can be approximated to the volume of a sphere of radius h. Therefore, for our data, the droplet height scales with the volume as:

$$h \sim \Omega^{1/3}\,. \tag{6}$$

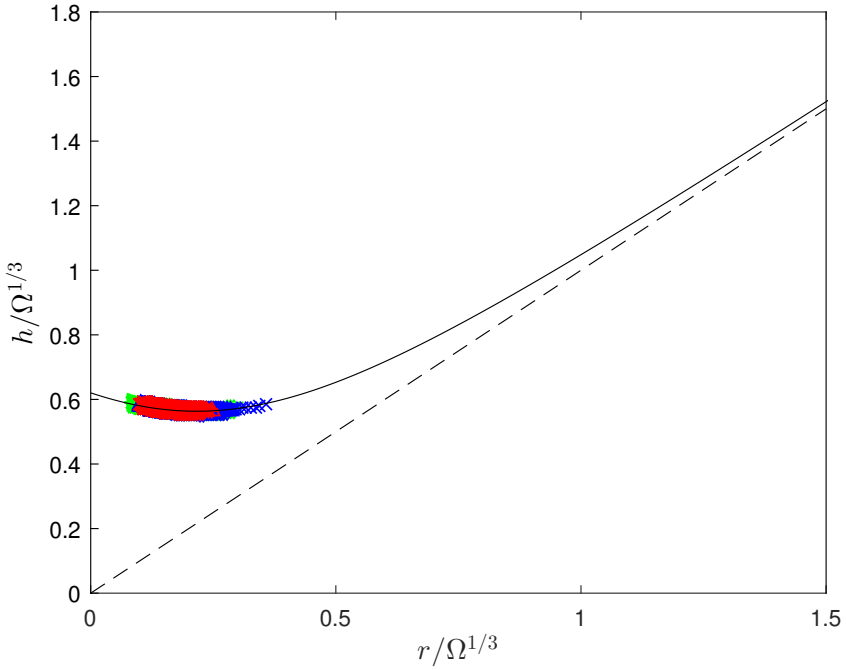

FIG. 3. The reduced height $h/\Omega^{1/3}$ of all studied droplets plotted as a function of the reduced radii of the fibers $r/\Omega^{1/3}$, on which the droplets are migrating. The markers show the experimental data of all studied droplets. The different colors for the markers are for the different viscosities of our experimental data: 1000 cSt (red), 2000 cSt (green) and 5000 cSt (blue). The solid black line represents the theoretical relationship between $h/\Omega^{1/3}$ and $r/\Omega^{1/3}$, as derived by Carroll [14, 15]. The dashed black line of equation $h = r$ shows that the predicted h tends towards r for large fiber radii.

The relationship of Eq. 6 can be verified as done in Fig. 4, which displays the average value of h as a function of Ω on a logarithmic scale for all studied droplets. The slope of the drawn line is $1/3$ as expected. Consequently, if the volume of droplets is controlled when they are produced, their speed v can be predicted as a function of only externally fixed parameters. Substituting Eq. 6 back into Eq. 5, a final expression for v can be written as:

$$v \sim \frac{\gamma}{\eta} \frac{\Omega^{1/3}}{r} \frac{dr}{dz} \,. \tag{7}$$

IV. DISCUSSION

It is now necessary to check if this model is in good agreement with the experimental data. To do so, Eq. 7 is rewrittten as:

$$\frac{v}{\Omega^{1/3}} \sim \frac{\gamma}{\eta} \frac{1}{r} \frac{dr}{dz} \,. \tag{8}$$

If the left term of Eq. 8 is plotted against $\frac{1}{r}\frac{dr}{dz}$, then it is expected that the data should follow a straight line through the origin with a slope proportional to $\frac{\gamma}{\eta}$. The corresponding experimental data is displayed in Fig. 5(a) for all the studied droplets (52 in total). The experimental data is in excellent agreement with the model. The droplets follow three different trends that represent the three different viscosities: 1000 cSt (red markers centered on the dashed line), 2000 cSt (green markers centered on the dotted line) and 5000 cSt (blue markers centered on the solid line). For each viscosity, three different fibers of varying radii and gradients were used to diversify the experimental conditions. They correspond to the different colors shades of the markers. On each single fiber, several droplets migrations (6 on average) were recorded once the fiber was pre-wet. In Fig. 5(a) each different type of marker stands for a different droplet. According to Eq. 8, these straight lines have slopes that are inversely proportional to the respective viscosities of the fluids but otherwise have the same prefactor. The prefactor itself is the result of the multiplication

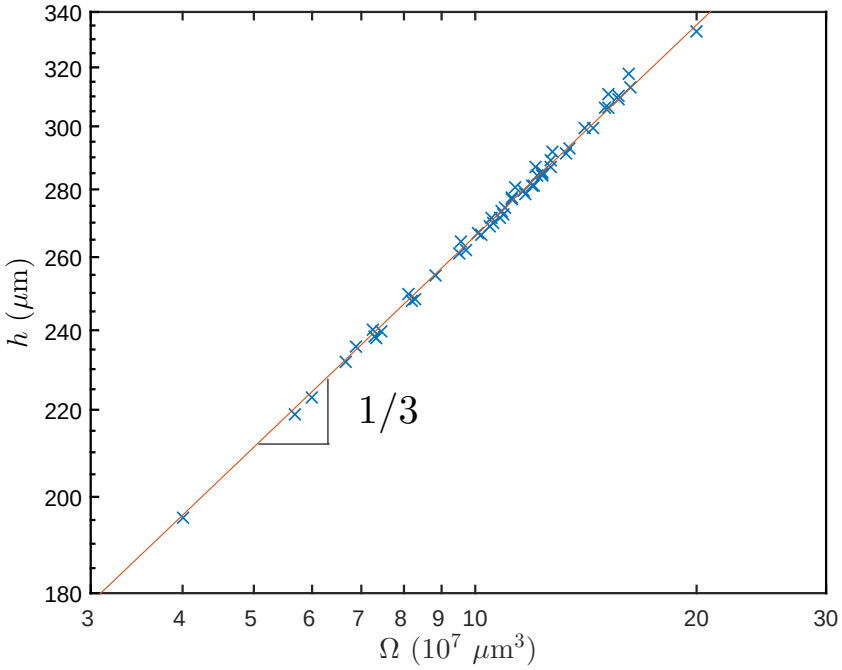

FIG. 4. The average height of all studied droplets plotted as a function of their volume on a log-log scale. The data is described by a line of slope 1/3.

of the surface tension γ (the same for the three oils that were used) and a numerical coefficient.

The comparison between model and data can be facilitated even further by multiplying the left term of Eq. 8 by the viscosity of the oil. In other terms, this operation allows for a normalization of all data by the corresponding viscosities. The expectation is then to obtain a single trend for all droplets, in this case a straight line going through the origin with a slope equal to the prefactor discussed earlier: the product of γ and a numerical prefactor which we find to be equal to 0.04 by fitting the data. We see in Fig. 5(b) that all data collapse onto the solid black straight line. The agreement between the data and the model further demonstrates the robustness of the model.

Furthermore, the limits of the model which were discussed in the previous section were also observed in the experiments. For instance, when the droplet continues to migrate towards the larger end of the fiber, there is a point where the relationship $h \gg r$ no longer holds. Therefore, there is a deviation of the data from the expected straight line when plotted as in Fig. 5(b): after following the line, the plot of the experimental data flattens and reaches a constant value. Similarly, when the droplets are too small, the condition $h \gg r$ is not satisfied, and the same deviation is observed. Failure of our model can also be observed for droplets with extreme volumes. When the volume is sufficiently large, gravity cannot be neglected, and the droplet motion deviates from the expected behaviour. This deviation happens when the characteristic dimension of the droplet is larger than the capillary length.

An interesting observation can be made about the first droplets to migrate on each fiber, as these are moving on a dry fiber. The resulting data for these droplets also collapse onto a straight line going through the origin when plotted as in Fig. 5(b). The only difference is that the slope of this line is different from the slope of the wet fiber data by a factor of approximately 4. The altered dynamics is because the absence of a pre-wetting film increases the viscous dissipation at the advancing contact line but also introduces modifications to the driving force depicted in Fig. 1(b). However, as expected, the overall scaling remains unchanged.

The work presented here differs from the work done by Lorenceau and Quéré in 2004 [16] and the work by Li and Thoroddsen in 2013 [21] in several ways. First, in our experiments, gravity is negligible because we consider droplets with characteristic sizes smaller than the capillary length, while Lorenceau and Quéré studied larger droplets. Second, here we focus on a broad range of relative droplet sizes in the quasi spherical regime. In contrast, Lorenceau and Quéré focus on experimental results in the quasi cylindrical regime. Third, our theoretical model differs from the

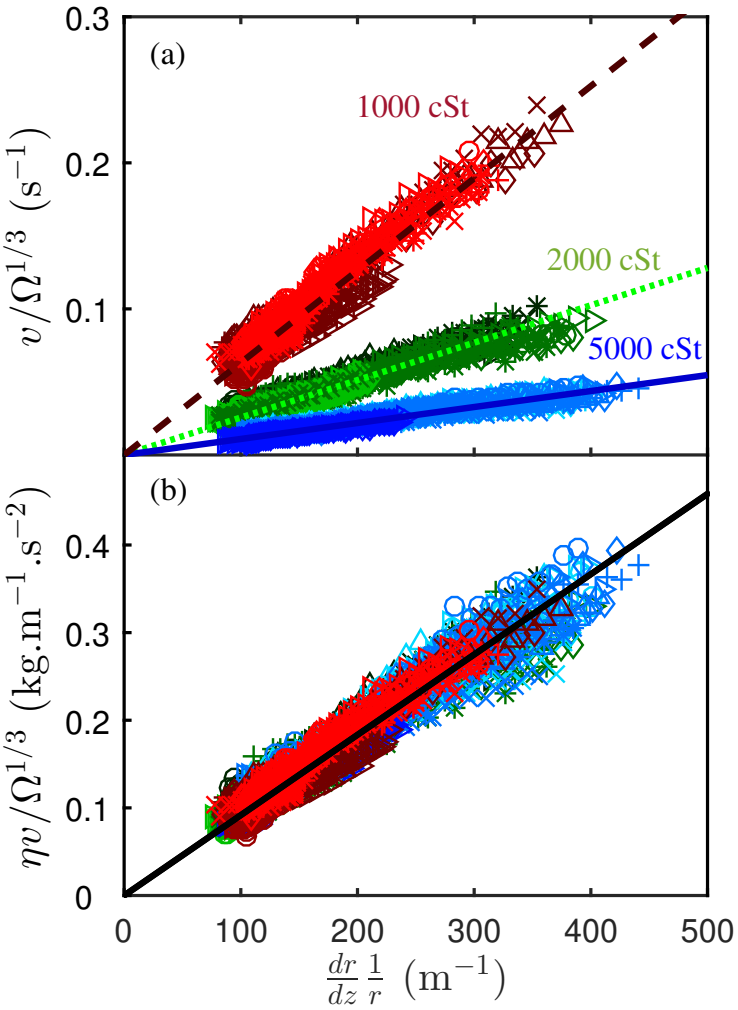

FIG. 5. (a) Speed normalized by the volume to the power of 1/3 for all studied droplets as a function of the gradient of their respective fibers divided by their radii. The main different colors represent the viscosity of the PDMS: 1000 cSt (red markers centered on the dashed line), 2000 cSt (green markers centered on the dotted line) and 5000 cSt (blue markers centered on the solid line). The different shades of these colors denote different fibers (3 different fibers for each viscosity). The different types of markers represent the different droplets. The lines represent the expected trends for each viscosity with a slope proportional to γ/η. (b) Speed normalized by the volume to the power of 1/3 and multiplied by the viscosity for all studied droplets as a function of the gradient of their respective fibers divided by their radii. The color scheme is the same as in Fig 4(a). The straight line represents the expected trend for all droplets with a slope proportional to γ.

model built by Lorenceau and Quéré and used by Li and Thoroddsen. We also predict the droplet speed using a balance of both the viscous dissipation and the driving force, but use a different approximation for the dissipation and define our driving force through the tensions at the contact line. Furthermore, in previous works by Lorenceau and Quéré and Li and Thoroddsen, even if experimental data is shown to collapse onto straight lines, none of these lines go through the origin, as would be expected if their model applied. The discrepancy between the model and the data suggests that our model brings improvement to the prediction of the speed of a droplet on a conical fiber.

V. CONCLUSION

In this work, the spontaneous migration of a droplet on a fiber with a radius gradient has been characterized. If gravity and inertia are negligible, and the droplet height much exceeds the fiber radius, the speed of the droplet can be predicted as a function of the other parameters of the system. These parameters are geometrical (radius and gradient of the fiber, droplet volume) and fluid characteristics (viscosity, surface tension). This prediction is based on a simple theoretical model in which the viscous shear force on the droplet balances the surface tension driving force.

We find a good agreement between this model and a large number of experiments that were performed using various fiber shapes and droplet volumes. Therefore, one could imagine using this model to improve future fog harvesting devices inspired by this spontaneous droplet migration mechanism.

ACKNOWLEDGMENTS

The authors are grateful to Michael Brook and Dan Chen for providing the silicon oils and for valuable discussions. The financial support by the Natural Science and Engineering Research Council of Canada is gratefully acknowledged.

[1] Q. Wang, X. Yao, H. Liu, D. Quéré, and L. Jiang, Proc. Natl. Acad. Sci. USA **112**, 9247 (2015).
[2] C. Duprat, S. Protiere, A. Beebe, and H. Stone, Nature **482**, 510 (2012).
[3] Y. Zheng, H. Bai, Z. Huang, X. Tian, F.-Q. Nie, Y. Zhao, J. Zhai, and L. Jiang, Nature **463**, 640 (2010).
[4] A. R. Parker and C. R. Lawrence, Nature **414**, 33 (2001).
[5] Z. Pan, W. G. Pitt, Y. Zhang, N. Wu, Y. Tao, and T. T. Truscott, Nat. Plants **2**, 16076 (2016).
[6] J. Ju, H. Bai, Y. Zheng, T. Zhao, R. Fang, and L. Jiang, Nat. Commun. **3**, 1247 (2012).
[7] L. Guo and G. Tang, Int. J. Heat Mass Transf. **84**, 198 (2015).
[8] C. Luo, Langmuir **31**, 11809 (2015).
[9] K. Li, J. Ju, Z. Xue, J. Ma, L. Feng, S. Gao, and L. Jiang, Nat. Commun. **4**, 2276 (2013).
[10] J. Ju, K. Xiao, X. Yao, H. Bai, and L. Jiang, Adv. Mater. **25**, 5937 (2013).
[11] X. Heng, M. Xiang, Z. Lu, and C. Luo, ACS Appl. Mater. Interfaces **6**, 8032 (2014).
[12] Y. Peng, Y. He, S. Yang, S. Ben, M. Cao, K. Li, K. Liu, and L. Jiang, Adv. Funct. Mater. **25**, 5967 (2015).
[13] M. Cao, J. Ju, K. Li, S. Dou, K. Liu, and L. Jiang, Adv. Funct. Mater. **24**, 3235 (2014).
[14] B. Carroll, J. Colloid Interface Sci. **57**, 488 (1976).
[15] B. Carroll, Langmuir **2**, 248 (1986).
[16] É. Lorenceau and D. Quéré, J. Fluid Mech. **510**, 29 (2004).
[17] S. Michielsen, J. Zhang, J. Du, and H. J. Lee, Langmuir **27**, 11867 (2011).
[18] L. Jian-Lin, X. Re, L. Bing-Wei, and F. Xi-Qiao, Chin. Phys. Lett. **24**, 3210 (2007).
[19] Y.-E. Liang, H.-K. Tsao, and Y.-J. Sheng, Langmuir **31**, 1704 (2015).
[20] X. Tan, T. Shi, Z. Tang, B. Sun, L. Du, Z. Peng, and G. Liao, J. Bionic Eng. **13**, 364 (2016).
[21] E. Q. Li and S. T. Thoroddsen, Phys. Fluids **25**, 052105 (2013).
[22] C. Lv, C. Chen, Y.-C. Chuang, F.-G. Tseng, Y. Yin, F. Grey, and Q. Zheng, Phys. Rev. Lett. **113**, 026101 (2014).
[23] M. Reyssat, L. Courbin, E. Reyssat, and H. A. Stone, J. Fluid Mech. **615**, 335 (2008).
[24] P. Renvoisé, J. Bush, M. Prakash, and D. Quéré, Europhys. Lett. **86**, 64003 (2009).
[25] J. W. Bush, F. Peaudecerf, M. Prakash, and D. Quéré, Adv. Colloid Interface Sci. **161**, 10 (2010).
[26] Z. Wang, C.-C. Chang, S.-J. Hong, Y.-J. Sheng, and H.-K. Tsao, Phys. Rev. E **87**, 062401 (2013).
[27] E. Reyssat, J. Fluid Mech. **748**, 641 (2014).
[28] É. Ruiz-Gutiérrez, C. Semprebon, G. McHale, and R. Ledesma-Aguilar, J. Fluid Mech. **842**, 26 (2018).
[29] J. Bico, B. Roman, L. Moulin, and A. Boudaoud, Nature **432**, 690 (2004).
[30] C. Duprat, J. M. Aristoff, and H. A. Stone, J. Fluid Mech. **679**, 641 (2011).
[31] J. M. Aristoff, C. Duprat, and H. A. Stone, Int. J. Non Linear Mech. **46**, 648 (2011).
[32] M. Taroni and D. Vella, J. Fluid Mech. **712**, 273 (2012).
[33] J. Bico, É. Reyssat, and B. Roman, Annu. Rev. Fluid Mech. **50**, 629 (2018).
[34] P. de Gennes, F. Brochard-Wyart, and D. Quéré, Capillarity and Wetting Phenomena: Drops, Bubbles, Pearls, Waves (Springer New York, 2003).
[35] R.-J. Roe, J. Colloid Interface Sci. **50**, 70 (1975).
[36] G. McHale, M. Newton, and B. Carroll, Oil Gas Sci. Technol. **56**, 47 (2001).

Chapter 4

Conclusion

The spontaneous migration of drops on conical fibers is a clever trick used by plants and animals to harvest water necessary to their survival. To mimic this spontaneous migration of drops in order to produce efficient water collectors, we need to understand the theory behind the migration. In the present work, we developed an experimental set-up that deliberately simplifies the drop on conical fiber system: we used silicone oil droplets which are more stable and less volatile than water droplets, and conical glass fibers which have a smooth surface unlike cactus spines. We also presented a theoretical model to predict the droplet speed and we tested this model in a range of droplet sizes and pipette geometries that has not thus far been tested. This droplet speed prediction model applies to situations in which gravity is negligible. The idea behind this droplet speed prediction model is that there is a balance between the two forces applied on the droplet: the driving force created by surface tension and the viscous dissipation at the solid liquid contact line. The model matches well with the droplet speed measured in our experimental set-up, even for different fibers of different sizes and gradients and also for different liquid viscosities.

To go further, we started a collaboration with Professor Carlson's group at the University of Oslo. This group is currently trying to simulate our droplet on conical fiber system to be able to confirm our model and also to explore extreme configurations that were difficult to reach experimentally (e.g. larger or smaller fiber radius gradients). We hope that the results of our collaborators and ours will help bring a

deeper understanding of the phenomenom and of the field of capillarity in general. Indeed, the knowledge gained aims to add to our understanding of a mechanism used in nature, not only for cactus spines, but also for spider webs, the beak of some birds species, the legs of water striders and many more. At a practical level, the present work can provide insight into ideal geometries for fog harvesting in arid environments and help build artificial fog collectors.

Bibliography

[1] Élise Lorenceau and David Quéré. Drops on a conical wire. *J. Fluid Mech.*, 510:29–45, 2004.

[2] P.G. de Gennes, F. Brochard-Wyart, and D. Quéré. *Capillarity and Wetting Phenomena: Drops, Bubbles, Pearls, Waves*. Springer New York, 2003.

[3] C Duprat, S Protiere, AY Beebe, and HA Stone. Wetting of flexible fibre arrays. *Nature*, 482(7386):510, 2012.

[4] Alban Sauret, François Boulogne, Katarzyna Somszor, Emilie Dressaire, and Howard A Stone. Drop morphologies on flexible fibers: influence of elastocapillary effects. *Soft matter*, 13(1):134–140, 2017.

[5] S Protiere, C Duprat, and HA Stone. Wetting on two parallel fibers: drop to column transitions. *Soft Matter*, 9(1):271–276, 2013.

[6] C Duprat and S Protiere. Capillary stretching of fibers. *EPL (Europhysics Letters)*, 111(5):56006, 2015.

[7] D Richard and D Quéré. Bouncing water drops. *EPL (Europhysics Letters)*, 50(6):769, 2000.

[8] R Kannan and D Sivakumar. Drop impact process on a hydrophobic grooved surface. *Colloids and Surfaces A: Physicochemical and Engineering Aspects*, 317(1-3):694–704, 2008.

[9] Rafael Schulman, John Niven, Michiel Hack, Christian DiMaria, and Kari Dalnoki-Veress. Elastocapillary wetting: Square holes and square droplets. *Bulletin of the American Physical Society*, 2018.

[10] Jie Ju, Hao Bai, Yongmei Zheng, Tianyi Zhao, Ruochen Fang, and Lei Jiang. A multi-structural and multi-functional integrated fog collection system in cactus. *Nat. Commun.*, 3:1247, 2012.

[11] Yongmei Zheng, Hao Bai, Zhongbing Huang, Xuelin Tian, Fu-Qiang Nie, Yong Zhao, Jin Zhai, and Lei Jiang. Directional water collection on wetted spider silk. *Nature*, 463(7281):640, 2010.

[12] Edward Yu Bormashenko. *Wetting of real surfaces*, volume 19. Walter de Gruyter, 2013.

[13] Henk Huinink. *Fluids in Porous Media*. 2053-2571. Morgan & Claypool Publishers, 2016.

[14] Arthur W Adamson, Alice Petry Gast, et al. Physical chemistry of surfaces. 1967.

[15] John Shipley Rowlinson and Benjamin Widom. *Molecular theory of capillarity*. Courier Corporation, 2013.

[16] Edward Armand Guggenheim. *Thermodynamics: An Advanced Treatise for Chemists and Physicists*. North-Holland Publishing Company, 1967.

[17] George Keith Batchelor. *An introduction to fluid dynamics*. Cambridge university press, 2000.

[18] David J Acheson. *Elementary fluid dynamics*. Oxford University Press, 1990.

[19] BJ Carroll. The accurate measurement of contact angle, phase contact areas, drop volume, and laplace excess pressure in drop-on-fiber systems. *J. Colloid Interface Sci.*, 57(3):488–495, 1976.

[20] BJ Carroll. Equilibrium conformations of liquid drops on thin cylinders under forces of capillarity. a theory for the roll-up process. *Langmuir*, 2(2):248–250, 1986.

[21] Glen McHale, MI Newton, and BJ Carroll. The shape and stability of small liquid drops on fibers. *Oil Gas Sci. Technol.*, 56(1):47–54, 2001.

[22] Ryong-Joon Roe. Wetting of fine wires and fibers by a liquid film. *J. Colloid Interface Sci.*, 50(1):70–79, 1975.

[23] Glen McHale, NA Käb, MI Newton, and S Michael Rowan. Wetting of a high-energy fiber surface. *J. Colloid Interface Sci.*, 186(2):453–461, 1997.

[24] Tung-He Chou, Siang-Jie Hong, Yu-En Liang, Heng-Kwong Tsao, and Yu-Jane Sheng. Equilibrium phase diagram of drop-on-fiber: Coexistent states and gravity effect. *Langmuir*, 27(7):3685–3692, 2011.

[25] Er Qiang Li and Sigurdur T Thoroddsen. The fastest drop climbing on a wet conical fibre. *Phys. Fluids*, 25(5):052105, 2013.

[26] Xianhua Tan, Tielin Shi, Zirong Tang, Bo Sun, Li Du, Zhengchun Peng, and Guanglan Liao. Investigation of fog collection on cactus-inspired structures. *J. Bionic Eng.*, 13(3):364–372, 2016.

[27] Cheng Luo. Theoretical exploration of barrel-shaped drops on cactus spines. *Langmuir*, 31(43):11809–11813, 2015.

[28] Brendan Joseph Carroll. Droplet formation and contact angles of liquids on mammalian hair fibres. *Journal of the Chemical Society, Faraday Transactions 1: Physical Chemistry in Condensed Phases*, 85(11):3853–3860, 1989.